Title

Hurry Up and Wait: Managing the Inherent Mismatches in Time Scales in Natural and Artificial Photosynthetic Systems

Journal

ACS Catalysis, 13(11)

ISSN

2155-5435

Authors

Houle, Frances A

Yano, Junko

Ager, Joel W

Publication Date

2023-06-02

DOI

10.1021/acscatal.3c00355

Hurry Up and Wait:

Managing the Inherent Mismatches in Timescales in Natural and Artificial Photosynthetic Systems

Frances A. Houle,[a,b,c*] *Junko Yano,*[b] *and Joel W. Ager*[c,d,e]

[a]Liquid Sunlight Alliance, Lawrence Berkeley National Laboratory, Berkeley, California 94720, United States

[b]Molecular Biophysics and Integrated Bioimaging Division, Lawrence Berkeley National Laboratory, Berkeley, California 94720, United States

[c]Chemical Sciences Division, Lawrence Berkeley National Laboratory, Berkeley, California 94720, United States

[d]Materials Sciences Division, Lawrence Berkeley National Laboratory, Berkeley, California 94720, United States

[e]Department of Materials Science and Engineering, University of California, Berkeley, Berkeley, CA 94720, United States

*Author to whom correspondence should be addressed: fahoule@lbl.gov

Keywords: natural photosynthesis, artificial photosynthesis, catalysis, kinetics, electrochemistry, enzymes

Abstract

Because single catalysts cannot selectively convert CO_2 into a specific reduced product more complex than CO either electrochemically or photoelectrochemically, an alternative is to use multiple catalysts organized into a cascade, which offers a means of generating complex chemicals with improved specificity by providing a channel for CO and similar intermediates to be reduced further. The rules for how to select catalysts for this purpose and design systems that have a high degree of chemical control using them are not known however. The efficiency and selectivity for individual catalysts may be optimized, but the resulting efficiency of an entire system will depend on how well the timings of all the chemical steps in the cascade as well as transport between the catalysts are managed. In this Perspective we discuss these challenges, and examine the ways in which control is exerted in natural photosynthetic systems which use cascaded reactions to convert CO_2 from the air into sugars using sunlight as the sole source of energy. These cascades take place within complex architectural elements that ensure that the chemistry is as efficient as possible. Adaptations of the functions of these natural design elements to artificial systems may offer ways to attain the promise of artificial photosynthesis.

Introduction

Both natural and artificial photosynthesis to convert CO_2 and H_2O into complex products using sunlight as a source of energy involve a sequence of reaction steps taking place at various

locations that are spatially distributed in the system. In all architectures, energy to drive chemical reactions is provided by a Z-scheme sequence of excitations and electron transfer events[1,2] leading to reduction and oxidation reactions that take place in separate regions. Natural systems rely on Photosystem I (PSI) and Photosystem II (PSII) to deliver energy, while artificial systems most commonly use dyes,[3] nanoparticles[4,5] and semiconductors.[2] Z-scheme hybrid electrodes containing PSI or PSII photoabsorbers have been reported.[6,7] Whether natural or artificial, these reactions require transport of protons and electrons to reduction centers. Simple implementations of the Z-scheme as developed for H_2 generation by water splitting in artificial systems by incorporating suitable electrodes and photocatalysts are not enough to realize the full power of natural designs, however. Natural (photo)catalytic sequences involve complex systems of enzymes and redox shuttles in aqueous environments and in membrane walls, where each molecule performs one or more in a series of chemical steps to convert chemicals selectively from one form into another. Within the chloroplast, a sugar is synthesized using a sequence of 2-electron steps, using a 3-CO_2 process involving NADPH and ATP. Artificial systems are not as complex – most commonly they involve providing a single catalytic site (molecular or heterogeneous) that takes protons and electrons from water oxidation and uses them to directly reduce CO_2 through a sequence of steps that may include C-C couplings.[8,9] Single catalytic sites in artificial systems are not capable of performing the reduction transformations required to convert CO_2 both selectively *and* efficiently into sugars in natural systems, or, as numerous studies have made clear,[10–17] into hydrocarbons and oxygenates.

Systems with a much higher level of sophistication could in principle be designed for highly efficient and selective artificial photosynthesis under diurnal solar irradiation,[18–21] however

the rules for how to do so beyond important considerations of molecular energetics and structure – spatial and temporal arrangements at the meso and macro scales, selection of materials and chemistries for each step in a sequence at the nanoscale, how to combine light-driven and dark reactions - are not well developed. There are many degrees of freedom to optimize concurrently, which cannot be done by intuition. A useful strategy to move systematically toward such a design is to start from a performance target and identify the key system characteristics that must be present for that target to be met. This process is known as inverse design in the field of optics, where the necessary characteristics are determined mathematically.[22] Not enough is known about artificial photosynthesis to have mathematical models that can perform a similar function. The thought process of inverse design can be applied however, where starting from a performance target we can identify which essential system elements need to be present for the target to be reached. As illustrated in **Figure 1**, we can work progressively from the system scale toward smaller scales and eventually to the molecular level to specify the nature of the elements required at each scale and how they need to work together. This process quickly reveals what we already know how to do, and science gaps and opportunities for new ideas and innovative thinking. If we were to start from the molecular scale and work toward the system scale, many potential combinations of system elements are a priori possible at each step, making discovery of a few best ways very challenging.

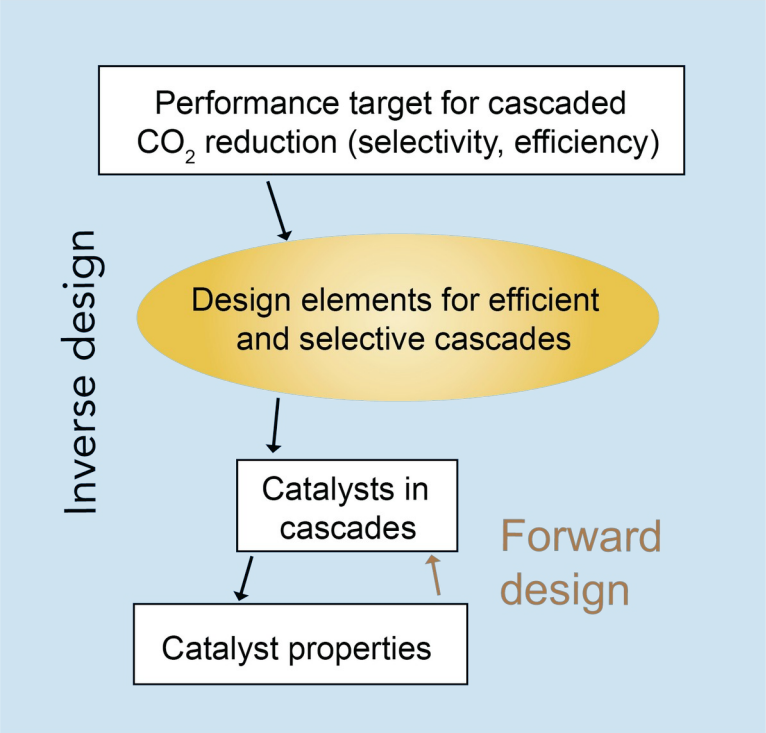

Figure 1. Schematic of processes that can be used to identify a successful research strategy meet a performance target at the system level. In the inverse design process, designated using black arrows, the process starts with the target and works from the system scale to the component scale (specific catalysts), defining specific requirements needed to meet the target at each step and simplifying the design space. The forward design process (gold arrow) starts at the component scale and works toward the system scale. This requires exploration of a rapidly expanding set of combinations of possible options at each stage to find the best few that might meet the performance target. Such a research scope becomes impractically broad for more than one or two stages when no obvious system constraints are identified by starting at the component scale. Both forward and inverse processes reveal that knowledge of design elements for efficient and selective cascades and how to implement them is lacking, however. Biological functions provide inspiration for overcoming this gap.

Applying the inverse process to determine useful design principles for artificial photosynthesis, we start from a target of selectivity as high as is found in nature, and improved efficiency relative to natural systems. There are many ways to think about how to reach this

target when involving artificial photosynthetic systems. In this Perspective we consider specifically how to design systems for CO_2 conversion into hydrocarbon and oxygenate products that do not require that a single catalytic site be made capable of meeting the target. This reveals immediately a major science gap as illustrated by the oval in **Figure 1**: we recognize that ideal catalytic cascades are required but do not know how to design them. We can list their required properties, however. In an ideal cascade, there should never be timescale mismatches among rates of light absorption and reaction by the components of the catalytic system, that is, no part of the system should ever be idle. This means that all aspects of the cascaded system are important and must be intentionally chosen so that reaction sites are able to function together like clockwork. This is a very tall order. Because of the native stochastics associated with any specific step involving one catalytic center,[23–25] the exact timings of steps cannot be predicted.

Assembling such steps into an efficient reaction sequence requires that active control of their timings be possible so that the uncertainty in how long each step will take is reduced to a minimum, and that there be ways to accommodate or buffer fluctuations.[23] This is another science gap. Two-step sequences that have been described for artificial inorganic systems involve transport of products from a catalyst in one region via flow or diffusion to another region, where further reaction can take place.[15,17,26–29] Both electrochemical and thermal catalytic schemes have used spatial strategies including integration of two catalysts to promote spillover, and incorporation into metal organic or porous aromatic frameworks to confine the intermediates during hydrogenation of CO_2.[30–33] While mass transfer between catalytic regions is clearly an essential process, it is only one of a number of elements that must be considered. Well-designed

cascades will fine-tune individual local concentrations and catalytic site densities, avoiding bottlenecks. This means we must learn to control all aspects of the system at all points in time – local concentrations, rates of diffusion of reactants and products, local molecular densities, excitations and energy transfer. Detailed experimental studies will be invaluable to identify the useful control points, and multiscale kinetic modeling (using stochastic techniques to capture the influence of fluctuations) will help develop a full picture of the system's evolution.

This leads us to consider the nature of the catalytic reaction itself and how it operates in a sequence. Whether natural or artificial, catalytic sequences constitute an overall catalytic cycle that has well-defined starting and ending points. The cycle will generally involve several subcycles, each having a range of chemical reaction rates at the cycle level and at the elementary step level. These rates control the overall efficiency of the sequence. How can artificial photosynthetic sequences that are designed to be selective to a specific product be designed at the same time to generate that product efficiently? Ideally, all the steps in the subcycles and overall cycle for the catalytic sequence will be fully coordinated among themselves, and operate at the maximum frequency possible. This places specific requirements on spatial layouts of the catalysts in the sequence, so that local reaction rates and transport between the sites are well-controlled. More typically, as illustrated in **Figure 2**, the overall transformation process involves steps that have a wide range of native timescales and are essentially uncoordinated in artificial photosynthesis. The transport of reactive intermediates and charge carriers, and the status of the catalytic cycles, must operate as a system in order for the sequence to be efficient.

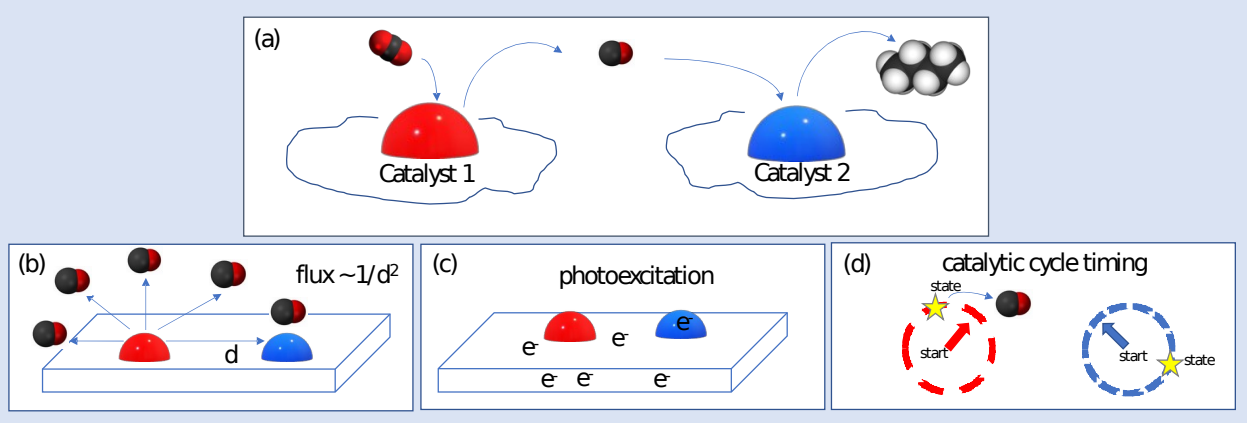

Figure 2. Sketch of the elements of a photo-driven catalytic cascade, illustrated for conversion of CO_2 on a surface to form higher hydrocarbons. (a) Two-step cascade using CO as an intermediate species. (b) Diffusive transport of CO between 2 catalytic centers, including isotropic desorption of CO over 2π steradians from Catalyst 1, and reduction of the flux directed toward Catalyst 2 according to the distance d separating them. (c) Arrival of continuously photogenerated electrons to drive the reduction reactions at Catalysts 1 and 2. (d) Illustration of how the states of the catalytic cycles for Catalysts 1 and 2 are unsynchronized, so that Catalyst 2 may not be ready to react with the intermediate CO when Catalyst 1 arrives.

How should the catalysts be selected for the sequences? The most common consideration is that each chemical step in the sequences has the lowest possible energetic requirement. To go from energetics to reaction rates, catalytic cycles that involve sequential charge transfer and chemical steps, such as those in (artificial) photosynthetic systems, are evaluated in terms of the free energies required for each of the steps as well as their free energies of activation. An energetically downhill sequence of steps is viewed as being more likely than an energetically uphill sequence.[34] Each step in the cycle will have a characteristic instantaneous rate, and the overall turnover frequency of the cycle is assumed to be controlled by steps that are endothermic or have a significant free energy of activation. While the energetic landscape is highly informative it is not all that is needed for sequence design: the importance of dynamic

heterogeneity, surface and fluid phase populations, and kinetic, rather than thermodynamic, control is becoming more widely appreciated.[35,36]

Having now considered artificial photosynthesis from an inverse design perspective, starting from the overall target down to the catalyst level, we outline in this Perspective how some rules for constructing useful artificial photosynthetic systems starting from what we know today might look. This involves working from catalyst to cascade in a forward design process as shown in **Figure 1**. We start with an evaluation of the connections between energetics and reactivity in complex catalytic reactions for a single center, and examine a simple case for how two centers might be coupled. When this point is reached, it is not clear from forward design what can be done next at a molecular level or systems level to ensure that the target of high selectivity and efficiency can be reached. Through inverse design we recognize that the central challenge is control over timing. New artificial photosynthesis design paradigms are needed to progress, and we return to natural photosynthetic systems to consider how they recruit spatial hierarchies and internal signaling as design principles. Drawing on these examples, we discuss possible non-biological approaches to incorporating these elements.

Evaluating the kinetics of the catalytic cycle at a specific center

To design efficient cascades, knowledge of the factors that influence the overall turnover rates and reaction rates for individual steps at each center is key: for separate centers to be coupled the reactive intermediate connecting them must be present at the right time to participate

in the chemistry. As a first step, let us consider the cycle at just one center in a cascade. It is tempting to identify a single rate determining step (RDS) as a proxy for overall cycle timing, and use this step to assess how well coupled cycles are coordinated. How to do this in a general and robust way is not straightforward, however, because the relationship between the concept of a rate determining step and the actual kinetics is complex.[37] In this section we discuss ways of identifying factors that control overall catalytic cycle rates at a single center. These methods are useful for diverse situations and show that energy landscapes alone are insufficient to determine the cycle rate. It is equally important to gain an understanding at each point in time of which steps are kinetically significant, and what the populations of reactants and intermediates involved in the chemistry are.

Quantifying rates. It is useful to review the specific definitions of reaction and diffusion rates and reaction rate coefficients and diffusion coefficients for this discussion, as they are not always clearly distinguished in the literature. As an example, the rate R of a generic second order chemical reaction step

$$A + B \rightarrow C \quad (1)$$

is defined as:

$$R = k\,[A][B] \quad (2)$$

where k is a rate coefficient. Differentiating between rates and rate coefficients is important because they measure different things. A rate is dependent on the state of the system, while a rate coefficient directly represents the physics associated with a chemical step through connection to its energetics and entropy as described in Transition State Theory and Butler-Volmer theory, or can be phenomenological, extracted by fitting experimental data according to an assumed mechanism. If the reaction step is an elementary step, one reactant (first order) or at most two

reactants (second order) are involved in the direct interaction leading to a chemical transformation. Higher order steps are often reported; however they are composite reactions because of the low probability of having 3 reactants meet and react simultaneously, and blend more than one elementary step.

Experiments designed to study an elementary reaction step allow an experimentally derived rate coefficient to be connected to a theoretical value calculated from the potential energy surface, revealing the nature of the chemical transformation in depth. For example, this connection can be made using kinetic Monte Carlo techniques combined with rate coefficients derived from theory for simple reactions where an individual reactant may have multiple possible reaction pathways.[38,39] Deriving a rate, which is the experimental observable, from a rate coefficient involves more than consideration of a single reactant, however, it requires knowledge of instantaneous populations of any species that can affect that rate. It cannot always be assumed that these populations (eg [A] and [B] in (**1**)) are at some constant value at all points in time in a system, which would result in the rate coefficient having a fixed proportion to the rate of a specific step. Moreover, a spatial distribution of [A] and [B] may be present, adding a requirement to integrate transport and intermolecular interactions into the reaction mechanism for the system.

Rate-determining step in zero dimensions (0D): photocatalysis. Following up on the discussion of the relationships between reaction rates and the concentrations/activities of reactant/products, we now turn to the determination of the RDS in a chemical network. By

definition, the RDS is that step for which changes in its rate has the largest influence on the overall conversion rate of the network. In a simple network of first-order reactions with no branching leading to a specific product, the RDS would be the step with the largest activation energy, E_a. However, this is not necessarily the case for more complex networks, such as those with second-order reactions, cyclic/looping elements,[40] or constraints arising from surface occupancy affecting the availability of reactants as are found in heterogeneous catalysis.[41,42]

Noting, as discussed below, that surface diffusion can add additional constraints, we begin with an analysis of the RDS in a prototypical photocatalytic reaction relevant to solar fuels: water oxidation on illuminated TiO_2. Water oxidation is closely coupled to reaction sequences involved in reduction reactions. We choose water oxidation on TiO_2 for three reasons. (1) It plays the same role as the water oxidation reaction that occurs in Photosystem II in natural photosynthesis, as discussed in the Nature-inspired Design Rules section, namely providing the electrons and protons which are used in coupled reduction processes. (2) There is better understanding of the elementary steps involved as a result of spectroscopic studies performed on metal oxides.[43,44] (3) As we will show, the RDS in this light-driven chemical network is not necessarily the one with lowest activation barrier.

We base our analysis on a simplified version of the microkinetic model (MKM) developed by Wang *et al.*,[45] **Table 1** and **Figure 3**. Note that this reaction mechanism considers proton and electron transfer separately and that it has a loop back in that two *O- species dimerize prior to the third transition state (TS3). Under conditions of solar illumination, assumed

to correspond to a normalized near-surface hole activity in the 10^{-10} to 10^{-9} range, a sensitivity analysis of their steady-state microkinetic model found that the turn over frequency (TOF) for OER is primarily determined by the rate with which photogenerated holes reach the surface; this has the interesting implication that if TiO_2 were to be p-type, such that holes, as majority carriers, could reach the surface, it would be an excellent OER electrocatalyst.

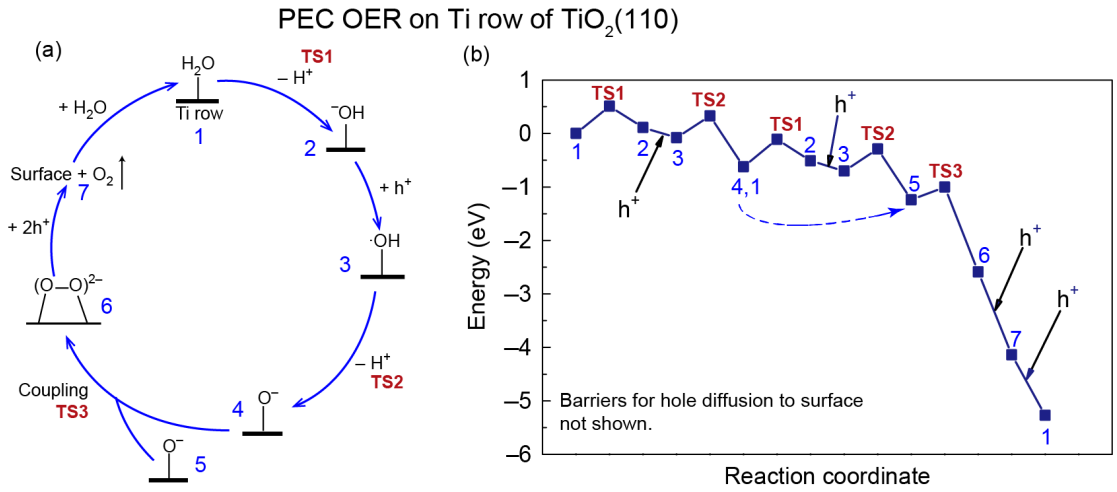

Figure 3. Simplified mechanism for photocatalytic OER on TiO_2(110). (a) depicted the sequence of steps and (b) shows the energy profile (see also **Table 1**). Note in (a) the that two *O- species must dimerize to create state 6 and that in (b) 4 and 5 couple yield state 6. Also, in (b), the barrier for hole capture associated is not depicted. Adapted with permission from Ref 45. Copyright 2018, Macmillan Publishers Limited.

Table 1. Energetics for PEC OER on TiO_2(110). For the three reactions involving holes, the activation barrier was envisioned to result from a barrier for near-surface hole to reach the surface. In addition, the model contains a barrier for near-surface holes to reach the surface. This barrier was used as an adjustable parameter (base case value of 0.25 eV) to assess the influence of hole activity on the overall rate of O_2 production.

Reactions	States[a]	ΔH (eV)	E_a (eV)
$H_2O(sol) + * \rightarrow *OH^- + H^+(sol)$	$1 \rightarrow 2$ (TS1)	+0.11	0.51
$*OH^- + h^+ \rightarrow *OH\text{-rad}$	$2 + h^+ \rightarrow 3$	-0.19	0.25
$*OH\text{-rad} \rightarrow *O^- + H^+(sol)$	$3 \rightarrow 4$ (TS2)	-0.54	0.41
$*O^- + *O^- \rightarrow *O_2^{2-} + *$	$5 \rightarrow 6$ (TS3)	-1.35	0.24

$*O_2^{2-} + h^+ \rightarrow *O_2^-$	$6 + h^+ \rightarrow 7$	-1.55	0.25
$*O_2^- + h^+ \rightarrow O_2(aq) + *$	$7 + h^+ \rightarrow 1$	-1.55	0.25

[a] States are shown in **Figure 3**.

It is interesting to consider which of the three chemical steps, denoted by TS1, TS2, and TS3 is rate-determining in this model. Further, the quantitative influence of the barrier for hole diffusion to the surface, involved in four of the steps ($2 + h^+ \rightarrow 3$ must occur twice), can also be evaluated. We suggest that the "degree of rate control" (DRC) concept introduced by Campbell is well-suited for this purpose,[46,47] noting that this methodology has been used extensively for the analysis of heterogeneous catalysis networks.[48–50] The DRC for an elementary step i of chemical network is defined as

$$X_{RC,i} = \frac{k_i}{R}\left(\frac{\partial R}{\partial k_i}\right)_{k_{j\neq i}, K_i} = \left(\frac{\partial \ln R}{\partial \ln k_i}\right)_{k_{j\neq i}, K_i} \quad (3)$$

where R is the overall rate leading to the target product and k_i is the rate coefficient for the i^{th} reaction. The derivative in Eq. (3) is computed by changing both the forward and reverse rate coefficient for the ith reaction in such a way as to leave the equilibrium constant K_i unchanged. If an Arrhenius form is used for the rate coefficient this can be simply accomplished via a small change in the activation energy for reaction i, leaving all other rate coefficients in the network unaltered. A reaction might have a DRC of 0 (its rate coefficient does not affect the overall reaction path or, equivalently, the step is kinetically insignificant). DRC is negative for a reaction which inhibits the overall rate. There are also cases where two steps exert rate control, having large DRCs that sum to nearly 1.

We now compute **(3)** for the microkinetic model shown in **Figure 3**. This is done numerically by making a small change in k_i for the ith reaction, recomputing all of the steady-state concentrations for the species in the model, recomputing the overall rate r, and computing the derivative in **Eq (3)** by finite differences. In this way, the effect of a change in the rate coefficient on all the concentrations in the network is captured. Application of this approach to photocatalytic water oxidation yields quantitative insights as shown in **Figure 4**, which depicts the DRC as function of near-surface hole concentration h^+ (a proxy for illumination level and expressed in units of fractional coverage), emphasizing again that holes are involved in four of the steps in **Table 1** ($2 + h^+ \rightarrow 3$ must occur twice). First, we note that at all hole concentrations TS3 (O-O coupling step with a barrier of 0.24 eV) does not influence the overall rate of O_2 formation. At low light excitation (relative hole activity ~10^{-10}), even though the barrier for water dissociation (TS1) is the largest in the chemical network, it has a lower DRC than either deprotonation of *OH (TS2) or hole diffusion,[51] which has the highest DRC. As the hole concentration increases, the influence of TS1 increases, becoming dominant at a hole concentration of 10^{-8} in fractional coverage units; this emphasizes the point made by Wang *et al*.[45] that the surface of TiO_2 is intrinsically active for OER. Further, this analysis clearly shows that examination of energy diagrams such as those depicted in **Figure 3(b)** is insufficient to assess the rate determining steps of a chemical network.

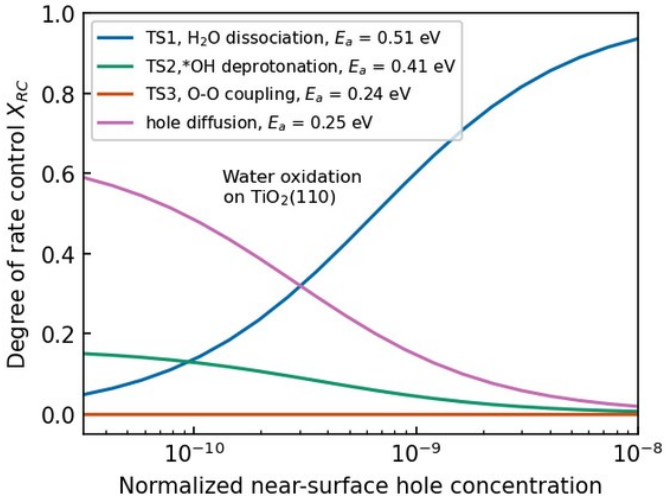

Figure 4. Degree of rate control in the chemical network of Wang *et al*. for photocatalytic OER on TiO_2(110). Hole diffusion to the surface is rate determining at low hole concentration while water dissociation is rate determining at higher hole concentrations.

Rate-determining step in 0D: electrocatalysis. We now turn to a case which is relevant to the cascades envisioned for CO_2 reduction. In many proposed cascades, CO is an intermediate. We illustrate the complexity of its kinetic landscape using the DRC concept discussed above to analyze the microkinetic model of Goodpaster *et al*.[52] for CO reduction on Cu(100). The model comprises the following elementary steps:

$CO(aq) + * \Leftrightarrow *CO$ (equilibrated) (R1)

$2\,CO* \Leftrightarrow *OCCO$ (R2)

$e^- + *CO \Leftrightarrow *CHO + OH^-(aq)$ (R3)

$*OCCO + *H \rightarrow *OCCHCO \rightarrow 2*$ (irreversible) (R4)

$*CO + *CHO \rightarrow *OCCHCO \rightarrow 2*$ (irreversible) (R5)

$H_2O(aq) \Leftrightarrow *H_2O$ (equilibrated) (R6)

$e^- + *H_2O \Leftrightarrow *H + OH^-(aq)$ (R7)

$e^- + *H + H_2O \rightarrow H_2 + OH^-(aq) + *$ (irreversible) (R8)

The *OCHCO species made (and desorbed) in **(R4)** and **(R5)** is thought to convert rapidly to C_2 compounds such as ethylene. By treating the electrolyte as a continuum dielectric, it was possible to capture the effect of the space charge field on the free energies of the intermediates and transition states. Potential dependent barriers were calculated for all the non-equilibrated steps and are illustrated in **Figure 5a**. Reactions **(R3)**, **(R7)**, and **(R8)** are electrochemical and, as expected, the barrier for the forward reaction decreases with at more negative applied potential. In contrast, the barriers for the forward reaction for the chemical steps, reactions **(R2)**, **(R4)**, and **(R5)**, increase with more negative applied potential. The model was designed to reproduce the differential electrochemical mass spectrometry results of Koper and co-workers, who found two peaks in the production of C_2 species as the potential was swept to more negative values.[53] Solving the system of non-linear algebraic equations for the steady-state surface coverages (**Figure 5b**) and partial current densities (**Figure 5c**) indeed shows that the model creates two pathways to C_2 species: one though hydrogenation of the *CO dimer (Reaction **(R4)**) and one, at more negative potential, via reaction of *CO and *CHO (Reaction **(R5)**), see the supporting information files for computational details.

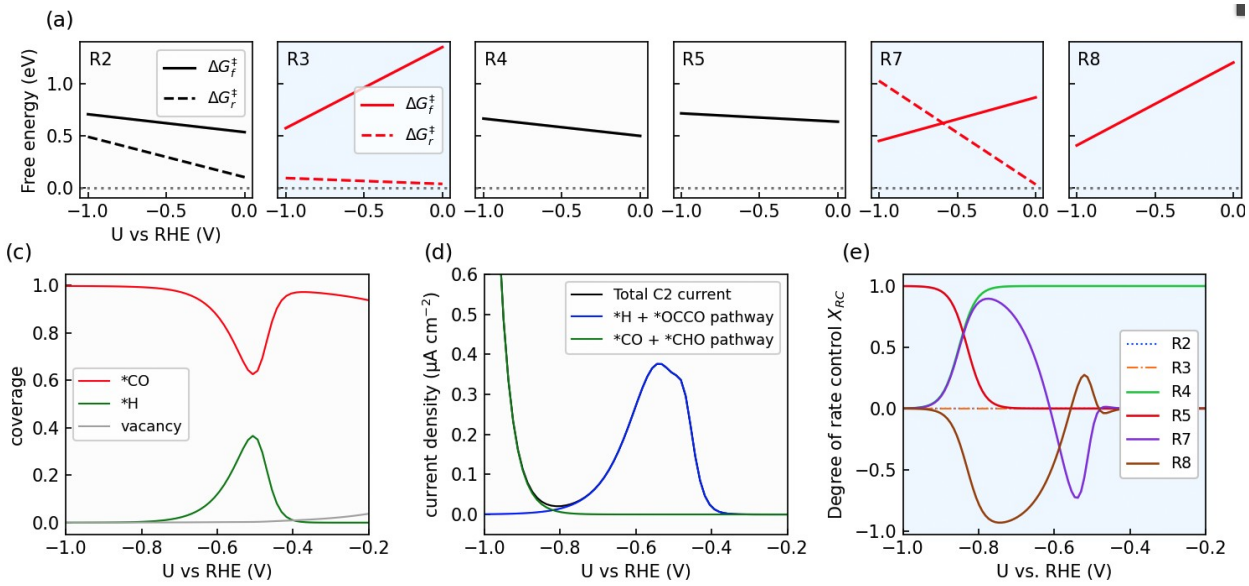

Figure 5. Degree of rate control in the chemical network of Goodpaster *et al*. for electrocatalytic reduction of CO on Cu(100): bulk pH = 7, surface pH = 9.5. (a) barriers for the non-equilibrated steps in the network: solid lines denote forward barriers and dashed lines denote reverse barriers. Chemical steps are indicated with black lines and electrochemical steps are denoted with red lines. Reactions **(R4)**, **(R5)**, and **(R8)** are irreversible in the model. (b) steady state coverages of *CO, *H, and empty sites. (d) partial current densities for the *OCCO pathway **(R4)** and *CO + *CHO pathway **(R5)**. (e) degree of rate control as a function of potential.

Examination of the DRC trends reveals further insights into the mechanism. At the point of current onset, -0.4 V vs. RHE, **(R4)** is rate-controlling, as one might expect. However, reaction **(R7)**, which populates the surface with hydrogen is inhibiting, having a negative value of X_{RC}. As the potential is swept to even more negative, **(R7)** switches to a promoting reaction (positive X_{RC}). Eventually, **(R5)** becomes rate-determining. It is notable that the rate constants for **(R2)**, *CO dimerization, and **(R3)**, proton-coupled electron transport (PCET) to *CO to form *CHO, have no influence on the overall rate of C_2 product production. This analysis is another example of how examination of barrier heights only is not adequate to assess the relative importance of elementary steps in a chemical network.

More generally, for all but the simplest reaction networks, an analysis of the rates (cf. **(2)**, these are the products of rate coefficients and the activities of the reacting species) is required in order to learn how to control product production, either for optimization of a single process or, as discussed below, for matching rates in a cascade process. The examples above are steady-state analyses where DRC was used to capture the sensitivity of the chemical network to changes in the rate constants of the individual steps with a unitless number between -1 and +1, with -1 being complete inhibition control, +1 being complete promotion control, and 0 being no effect. It would be possible to generalize the approach to systems with either or both of temporal and spatial heterogeneity by computing **(3)** at specific times or places in the system simulation.

Rate determining processes in coupled reaction-transport

The DRC analysis in the preceding section provides insights to the kinetics of certain types of catalytic cycles at a single site, but as noted in the Introduction is not easily extended using a forward design analysis to reactions involving multiple catalysts where the reactions are not necessarily at steady state and where the reactant populations are present in multiple phases and vary in time. This situation applies to sequential systems of catalysts involving reactants that are supplied by diffusion and are running in parallel, but must be coordinated to optimize efficiency by understanding their native turnover frequencies. Direct reaction-diffusion simulations using stochastic chemical kinetics[54,55] to model the fully coupled catalyst-electrolyte system is one useful alternative to DRC techniques for such complex forward design situations. Stochastic kinetics simulations are an exact solution to the master equation for a reacting

system,[54,55] which collects all the mechanistic steps that control the reaction, including chemical steps and transport.[56,57] The method does not use coupled differential equations to calculate the time history of a system, rather it is a type of kinetic Monte Carlo simulation that is propagated by random selection of probability-weighted reaction steps, where the probabilities are calculated by normalizing the rates for each step to the total of the rates for all steps. The simulation generates an absolute time base for comparison to experimental measurements such as product formation rate and current density, and does not require making assumptions about the existence of a steady state condition. The computational method can accommodate systems with a wide range of instantaneous rates, so-called stiff systems, that are generally not tractable using ordinary differential equation solvers, and are suitable for simulating systems whose kinetics are governed by fluctuations which in practice cannot be modeled using differential equations. In addition to a full history of the system in space and time, the method generates information on the instantaneous rates of each step in the mechanism as will be described below. In the time since the stochastic kinetics algorithm was first described in the literature, it has become widely adopted in biology especially, and is known as the "Gillespie algorithm".[58] It has continued to be developed as a foundation for modeling complexity efficiently for specific types of chemical reactions but there has been much less emphasis in published work on extending it to real 3-D physical systems. Advances have been described in the patent literature and in the documentation for the general-purpose Kinetiscope code package used here, however, enabling nonlinear chemistry, coupled reaction-diffusion, volume changes, more efficient simulations of rapidly maintained equilibria, electric fields and time-varying stimuli for example.[57,59–61]

In this section we show how the stochastic chemical kinetics method can be used to understand the factors that affect the rate of a catalytic cycle for the specific case of electrocatalytic and non-electrochemical (thermal) conversion of CO_2 by Cu into C_1 products, in competition with H_2 generation. We obtain direct information on which steps strongly influence the reaction, and identify dominant and rare reaction pathways involved in formation of specific products. This allows us to streamline the steps that are possible into an operational chemical mechanism, and characterize how it evolves in time within a full system.

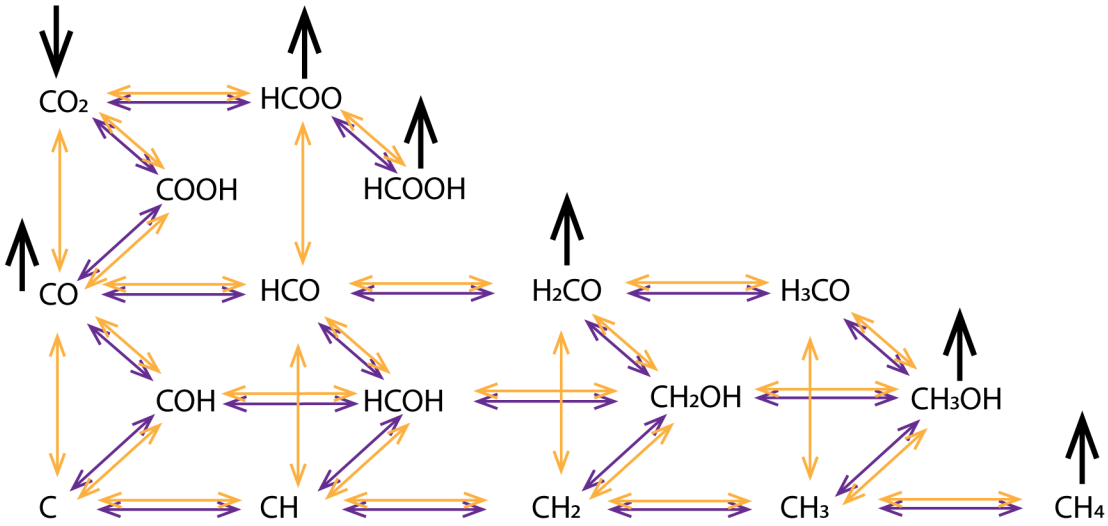

Scheme 1. Catalytic reaction network for CO_2 reduction on Cu to form C_1 products (hydrogen evolution reaction steps are not shown). Gold arrows are for non-electrochemical (thermal) steps, purple arrows are electrochemical steps, and black arrows are for adsorption of CO_2 (down) and desorption of products (up). Adapted with permission from Ref 62. Copyright 2020, The Authors. Published by Elsevier Ltd.

The simulations are set up using the reactions shown in **Scheme 1** for Cu (211) in contact with H_2O (see Supplementary Information for details). The rate coefficients for each step are calculated using corresponding thermal and electrochemical free energy data taken from a recent publication by Zijlstra, Hensen and coworkers.[62] We have added hydrogen evolution

reaction (HER) kinetics from Liu et al[63] to create a full model for CO_2 electroreduction in contact with a 0.1M HCO_3^- electrolyte (pH 6.8), whose major products are CH_4 and H_2 as determined by rotating disk electrode measurements. Using the open access stochastic kinetics simulation package Kinetiscope,[59] we model the reacting system in 2D as two disconnected 1 μm x 10 μm patches of catalyst with an overlayer of 147 μm of aqueous electrolyte, which includes CO_2-HCO_3^- and water dissociation chemistry.[64–70] An expanding spatial grid is used to capture nanoscale details in the electrolyte solution near the electrode surface while maintaining lower resolution in the bulk-like region. The free energy data are used to calculate rate coefficients using the Butler-Volmer expression

$$k = k_0 e^{-anF(E-E^0)/RT} \quad (4)$$

where k_0 is the standard rate coefficient calculated using the free energy of activation and transition state theory, α is the transfer coefficient and E^0 is the formal potential, calculated from the free energy of the reaction step. The starting conditions for the simulations assume the electrolyte is saturated with CO_2 (0.033 moles/L), and an initially bare Cu (211) surface with an adsorption site concentration assumed to be 3.2×10^{14} per cm^2. The applied potential is set to a value of -1.4V vs the standard hydrogen electrode (SHE).

In these simulations, the system's chemical composition evolves until steady state is reached. At steady state, the surface coverages by intermediate species do not change with time. However, the surface coverages of very reactive species can be zero most of the time because they are consumed as fast as they are produced – that is, they fluctuate. Under such conditions, a DRC analysis would not be possible since the reactant activities are zero, despite the fact that the

reactions do occur and play an important role in the reaction rate. The stochastic kinetics code package Kinetiscope[59] provides an alternative approach that is helpful to gauge reactivity in this common situation, which is to count selection frequencies, or numbers of occurrences per unit time as a proxy for rates. The event selection process works as follows. In order to simulate the time evolution of a chemical mechanism of n steps, the stochastic method uses the instantaneous rate R of a step i normalized by the sum of all R_i as a measure of probability P_i of that step occurring[54,55]

$$P_i = \frac{R_i}{\sum_{i=1}^{n} R_i} \tag{5}$$

The normalization ensures that each P_i is between 0 and 1. To select a reaction step, a random number Rn between 0 and 1 is generated, and the P_i added together until the total is > Rn. The ith step is then the one that occurs. The instantaneous value of the denominator in **(5)** is used to calculate the time step associated with this change in state of the system. When a step is selected, the stoichiometry of the step is used to update the reactant and product populations involved with that step, whether on the catalyst surface or in solution, the rates used in **(5)** are recalculated, and a new step selection cycle is launched. Steps with large values of P_i will be selected often, and those with smaller values will be selected more rarely. If a rate $R_i = 0$, which would be the case if the corresponding reactant population on the Cu surface is 0, then $P_i = 0$ and that particular step cannot be selected. However if the surface populations fluctuate, then the values for P_i involving those species will vary in time, and those steps can be selected occasionally. In Kinetiscope, all step occurrences during a simulation are tallied, enabling selection frequencies to be tracked using the simulation time base. These frequencies are analogous to a turnover frequency for a

particular reaction step, and can be taken to be proportional to the step's rate for the purpose of the present discussion.

If the energetics alone determined the rates of each step in the mechanism, then there should be a correlation between the rate coefficients determined using **(4)** and the selection frequencies of the more than 100 individual reaction steps. As can be seen in **Figure 6**, which collects data from all the elementary steps in the mechanism, there is no correlation between the free energy of activation and the selection frequency of a specific step, or between the rate coefficient at the applied potential and the selection frequency of a specific step. The full simulations of this mechanism provide detailed information on the individual reaction steps, only a few of which are found to be kinetically active in competition with HER. **Table 2** summarizes the results at about 0.1s, when surface coverages have become stable. It lists the selection frequencies for each step normalized to that for the CH_4 desorption step, and the corresponding reactant concentrations, rate coefficients and activation energies.

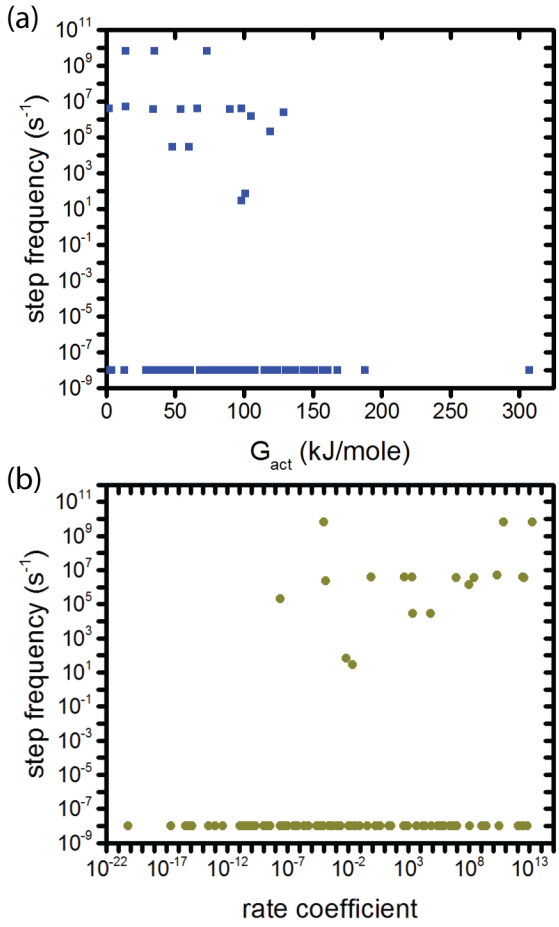

Figure 6. Trends in reaction step occurrence frequency in the mechanism for CO_2 reduction over Cu(211) at pH 6.8, -1.4V vs SHE, including all electrochemical and non-electrochemical (thermal) steps in Scheme 1. Frequencies of 0 (i.e. never selected) are set to 10^{-8} to include them on the log plots. (a) Frequencies as a function of free energy of activation from DFT calculations for the reaction step. (b) Frequencies as a function of rate coefficient calculated using Butler-Volmer theory for electrochemical steps and transition state theory for non-electrochemical (thermal) steps.

It is notable that the populations of most reactants are on average close to zero. The simulations show that the initial reduction step for CO_2 to COOH, **Table 2** step 1, is slow compared to CH_4 generation, **Table 2** step 15. Once CO is formed, there are two branches to generate adsorbed CH. One is CO → HCO → HCOH → CH, with a minor slow branch that

bypasses CH, HCOH → H_2COH → CH_2. The other is CO → COH → C → CH. The reaction to generate CH_4 from CH is fast. The steps in the HCO sequence have the same normalized selection frequencies as those for CH_4 formation, indicating that once HCO is formed the reactions are efficient, and reactive intermediates are rapidly consumed. The COH branch, on the other hand, is kinetically less active than the HCO branch, with slower formation of COH from CO and a buildup of adsorbed C. The presence of C enables a competing thermal reaction that converts C back to COH to occur. The coupled reaction steps 9 and 10 (**Table 2**) are highly probable, and compete effectively with reduction of C to eventually form CH_4. Thermal steps 2 and 10 (**Table 2**) produce surface-bound OH and H, respectively. The H (61% of the surface sites) can feed the HER reactions (not shown) while there is no clear fate for OH (31% of the surface sites) within the mechanism as described. Eventually the entire surface will be covered by OH and the reaction will stop. This indicates that the mechanism is incomplete, and that further development of its details will be important to gain an understanding of the catalytic cycle timing for CO_2 reduction chemistry.

Table 2. Rates coefficients for kinetically active steps in the CO_2 reduction mechanism on Cu (211) to form CH_4, and their predicted relative rates.

Step	Step selection rate relative to CH_4 desorption	Steady state reactant concentration (% of surface sites)	Rate coefficient	Ea (kJ/mole)
1. CO_2* + e- + H_2O → COOH* + OH-	0.62	0.017	1.41×10^{-4} cm/s	129
2. COOH* → CO* + OH*	1.30	a	2.17×10^{10} s^{-1}	14
3. CO* + e- + H_2O → HCO* + OH-	0.93	a	2.65×10^{8} cm/s	90
4. HCO* + e- + H_2O → HCOH* + OH-	0.93	a	3.51×10^{12} cm/s	54
5. HCOH* + e- + H_2O → CH_2OH* + OH-	0.008	a	4.82×10^{4} cm/s	48
6. HCOH* + e- → CH* + OH-	0.92	a	8.67×10^{6} cm/s	34

7. $H_2COH^* + e^- \rightarrow CH_2^* + OH^-$	0.008	a	1.86×10^{-5} cm/s	60
8. $CO^* + e^- + H_2O \rightarrow COH^* + OH^-$	0.37	a	9.65×10^{7} cm/s	105
9. $COH^* + e^- \rightarrow C^* + OH^-$	1659	a	1.77×10^{13} cm/s	35
10. $C^* + H_2O \rightarrow COH^* + H^*$	1659	8.60	6.88e10 s^{-1}. b	14
11. $C^* + e^- \rightarrow CH^* + OH^-$	0.05	8.60	2.41×10^{-8} cm/s	119
12. $CH^* + e^- + H_2O \rightarrow CH_2^* + OH^-$	0.98	a	438 cm/s	66
13. $CH_2^* + e^- + H_2O \rightarrow CH_3^* + OH^-$	0.98	a	0.84 cm/s	66
14. $CH_3^* + e^- + H_2O \rightarrow CH_4^* + OH^-$	1	0.001	1.69×10^{3} cm/s	98
15. $CH_4^* \rightarrow CH_4$	1	a	2.77×10^{12} s^{-1}	2

a. Steady state C-containing reactant populations are < 3 x 10^{-6} % of the surface site concentration
b. Pseudo-first order, assuming 3 H_2O per surface catalytic site

Just as was shown by the DRC analysis examined in the preceding section, the kinetics simulations and analysis of reaction rates show that examination of the free energy diagram leading from reactants to products and assuming that energetics alone determine reaction rates do not capture the full picture of how a catalytic cycle operates or what actually controls its cycle frequency even without considering that the catalytic site itself is not likely to be static. The picture of how electrons are consumed, the importance of thermal as well as electrochemical reactions, and which steps control the overall rate of CH_4 formation on Cu (211) emerges only from detailed simulations. Consideration of energetics alone does not predict the role of surface C, for example. It is important to appreciate that the steady state reactive intermediate concentrations can be very small, so instantaneous rates are governed by fluctuations rather than stable populations, and these fluctuations are pivotal in their influence on how the catalytic cycle progresses.

Cascaded artificial systems

The considerations about factors that affect rates and rate control at single catalytic centers discussed in the preceding section raise the question of how to construct catalytic

cascades that are efficient enough to meet our overall efficiency-selectivity target if the only information about their function is free energies of specific pathways. There is no direct way to connect the reaction energetics to the factors that control the cadence with which a catalytic center operates, such as reactant populations and transport processes to and from the catalytic center, which are essential to know to determine how a sequence of such cadences should be constructed. Without this knowledge, designing a sequence of cascaded catalytic reactions at different locations that operate optimally together, that is, where an intermediate released at one center can be utilized efficiently by another center because their catalytic cycles are compatible with each other and with the transport time, is clearly a major challenge. For example, without catalyst-to-catalyst coordination, even excellent optimization of one catalytic center in the cascade to form a desired intermediate may not be effective if downstream centers are not ready to begin their cycles when the intermediate arrives **(Figure 2d)**. The intermediates formed will have to remain nearby until the later catalytic processes catch up. This requires a mechanism for trapping them, otherwise they will diffuse away. The parameter space involved in coordinating a cascade is potentially vast: in this section we consider one case to begin to develop an appreciation for important reaction system characteristics.

Let us assume that we discover how to perfectly match separate catalysts in a two-step (photo)electrochemical cascaded sequence by control of kinetic rates throughout the catalytic cycles. Specifically, we find a way to provide exactly the same turnover frequency and rate controlling reaction steps in the reaction mechanism for both catalysts in a cascade even though the reactants and products are different. This could be done, for example, through control of

reactive surface areas in a system, or matching heterogeneous and molecular catalyst combinations. Is such a degree of coordination sufficient to allow optimization of a cascade?

The answer to this question depends on the turnover frequencies for the catalytic cycles in each catalyst of the sequence relative to time required for an intermediate species *I* to move between the first and second catalytic center according to the sequence's architecture. Assuming that the motion is governed by diffusion, the rate for this process between the centers in moles/vol-s is

$$R_D = D \nabla [I_{1-2}] A \qquad (6)$$

where *D* is the diffusion coefficient, $\nabla [I_{1-2}]$ is the concentration gradient of *I* between centers 1 and 2, separated by a distance *d*, and *A* is the cross-sectional area of the connecting volume directly in between the centers. *D* can vary over many orders of magnitude depending on the viscosity of the medium through which the intermediate moves, and how strongly the diffusant interacts with that medium through electrostatic or polar interactions. R_D can have a similar range depending on local concentration gradients, which are all-important to control the magnitude and directionality of the diffusant's flux. Steep gradients can drive efficient diffusion even when the diffusion coefficient is very small – for example, this is a key factor in determining nanometer-scale control over patterning in photolithography.[71] The value for *A* will depend on the overall architecture of the cascaded system. If the catalytic reactions are faster than transport of a substrate to both catalytic centers, then transport governs the local concentrations and the overall reaction rates.

It is clear that the spatial arrangement of the catalytic centers is critical, yet the rules for placement in artificial systems are not established. As a first guess, proximity of the reaction centers would seem to be very important.[27,29] The intermediate *I* passed between the catalytic centers can diffuse on the surface of the electrode, or detach, move through the electrolyte, and reattach: we can hypothesize that the smaller the distance, the more likely the transport coupling is likely to be efficient and effective. It should be noted that both modes of inter-center transport are often called spillover in the literature although the transport mechanisms (surface hopping vs diffusion in solution) and environmental requirements (availability of binding sites on both catalysts and solubility limits) are very different. To evaluate the importance of proximity, we create a simple 3-D model having a heterogeneous catalyst placement as shown in **Figure 7**. The model involves two cascaded heterogeneous catalytic regions immersed in an aqueous environment, having the same surface areas, and therefore numbers of individual catalytic sites within the region, and the same electrochemical reaction mechanisms. These regions are placed on a repeating grid, resulting in a range of inter-site distances. Diffusion between the catalytic centers is assumed to be through the electrolyte, via a detachment-reattachment process. Stochastic reaction-diffusion kinetics simulations as described in the preceding section for a 3-dimensional electrode-electrolyte system are used to address the specific question of whether or not proximity is key to overall efficiency in systems whose catalytic kinetics are fully matched.

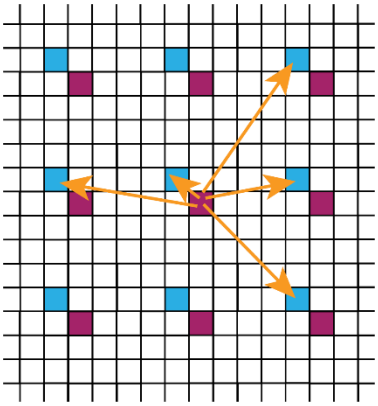

Figure 7. 2-catalyst sequential cascade model for electrochemical conversion of a reactant R into a product P. Catalytic region #1 (red) consumes R (dissolved in aqueous electrolyte) to produce an intermediate R2 which then diffuses through the electrolyte to react at Catalytic region #2 (blue) and form the final product. The dark green regions are the supporting substrate and are chemically inert, diffusion across them between sites does not occur.

We evaluate a hypothetical two step cascade that has the overall sequence, involving a catalytic site within the catalytic region.

Catalytic site #1 in region #1: Reactant $\rightarrow$ Intermediate reactant (R9)

Catalytic site #2 in region #2: Intermediate reactant $\rightarrow$ Product (R10)

To ensure a level of realism in the simulations, the catalytic chemical reactions involved for sites #1 and #2 are based on the heterogeneous 2-electron CO_2 reduction mechanism of CO_2 on Ag[72,73]

CO_2 (solution) + * $\Leftrightarrow$ CO_2* (R11)

CO_2* + e- $\Leftrightarrow$ COO-*+ H_2O $\rightarrow$ COOH* + OH- (R12)

COOH* + e- $\Leftrightarrow$ COOH-* + H_2O $\rightarrow$CO + * + OH- (R13)

where the rate coefficients for each of the steps **(R11)**-**(R13)** at the applied potential are determined using the free energies and the Butler-Volmer equation, **(4)**. The competing hydrogen

evolution reaction is omitted for simplicity, as is the full electrolyte chemistry for CO_2 saturated water containing 0.1M $KHCO_3$.

The steps **(R11)**-**(R13)** for Catalytic sites #1 and #2 are simplified as shown in **Table 3,** steps (1)–(3). *S* is the dissolved reactant that interacts with site #1 in region #1, SI_1 is an intermediate, and *I* is the product that desorbs to become $I_{1\text{-}2}$, which diffuses to site #2 in region #2 for further reaction. A parallel scheme at site #2 converts $I_{1\text{-}2}$ into the product *P*. The initial adsorption steps (1) for dissolved reactants *S* and $I_{1\text{-}2}$ are assumed to be controlled by a slow diffusive transfer step ($D = 10^{-10}$ cm^2/s) from the liquid to the catalyst surface reflecting the finding in the literature that adsorption onto Ag is inefficient due to rapid redesorption and the requirement for specific surface sites to be available.[73] The diffusion coefficients for *S*, $I_{1\text{-}2}$ and *P* are assumed to be $2x10^{-5}$ cm^2/s, typical for small molecule solutes in water.[74]

Table 3. Kinetics scheme used to simulate matched sites in a catalytic cascade.

Catalytic site #1	Catalytic site #2	Formal potential (V)	α	Standard rate constant (cm s^{-1})
(1) $S + * \Leftrightarrow S*$	(1) $I_{1\text{-}2} + * \Leftrightarrow I_{1\text{-}2}*$	--	--	--
(2) $S* + e^- \Leftrightarrow S*^- \rightarrow SI_1*$	(2) $I_{1\text{-}2}* + e^- \Leftrightarrow I_{1\text{-}2}*^- \rightarrow SI_2*$	0.03	0.5	0.241
(3) $SI_1* + e^- \Leftrightarrow I^{*-} \rightarrow I_{1\text{-}2} + *$	(3) $SI_2* + e^- \Leftrightarrow P^{*-} \rightarrow P + *$	-0.35	0.5	$2.16x10^{-7}$

For this scenario, the thickness of the aqueous liquid layer is 147 μm, the overall active surface area is taken to be 8% of the geometric area, with catalytic regions defined as shown in **Table 4**. The repeating grid results in a range of distances between pairs of Catalytic regions #1 and #2 as illustrated in **Figure 7**. It is important to note that when $I_{1\text{-}2}$ desorbs from Catalytic region #1 and diffuses away, its direction can be anywhere within a volume spanning 2π steradians from the

desorption site, resulting in a very small probability of diffusion in the specific direction of a site in Catalytic region #2, as illustrated in **Figure 2(b)**. This leads to a reduction in $I_{1\text{-}2}$ flux from site #1 to any site #2 with distance d between them of $1/d^2$.

Table 4. Heterogeneous catalyst characteristics

Case	Area of catalytic region (nm^2)	Number of catalytic sites in the region	Distance between pairs of regions (nm)
A	1	3	5
B	4	13	10
C	400	1264	100
D	40,000	126,441	1000

The simulation results for an applied potential of -1.4V vs SHE (pH = 6.8) are shown in **Figure 8** for Case D. The data show that in the time required to produce 0.25 moles/cm^2 of $I_{1\text{-}2}$ by Catalyst region #1, only $3x10^{-4}$ moles/cm^2 of P are formed even though Catalyst region #2 is immediately adjacent to #1. This is because $I_{1\text{-}2}$ cannot be directed from region #1 toward region #2: the reaction rate is too slow to build up a gradient to control diffusion in that particular direction. Since the rates at the two catalytic sites are matched, a concentration gradient from a site #1 in region #1 to site #2 in region #2 would never materialize and simple system flooding would be the only mechanism available to drive the overall cascade. The calculated rates can be used to estimate how much time it would take for $I_{1\text{-}2}$ and P to be produced at the same rate in this system, realizing the full rate matching that was intended. For the case of the total catalytically active area ~ 8% of the surface area, it would take about 40 minutes. If 96% of the area is catalytically active, it would take about 3.3 minutes. The fact that there is a time lag for

the two sites to reach equal reaction rates means that conversion of *R* into *P* can never be 100% efficient, there will always be residual $I_{1\text{-}2}$ in the system.

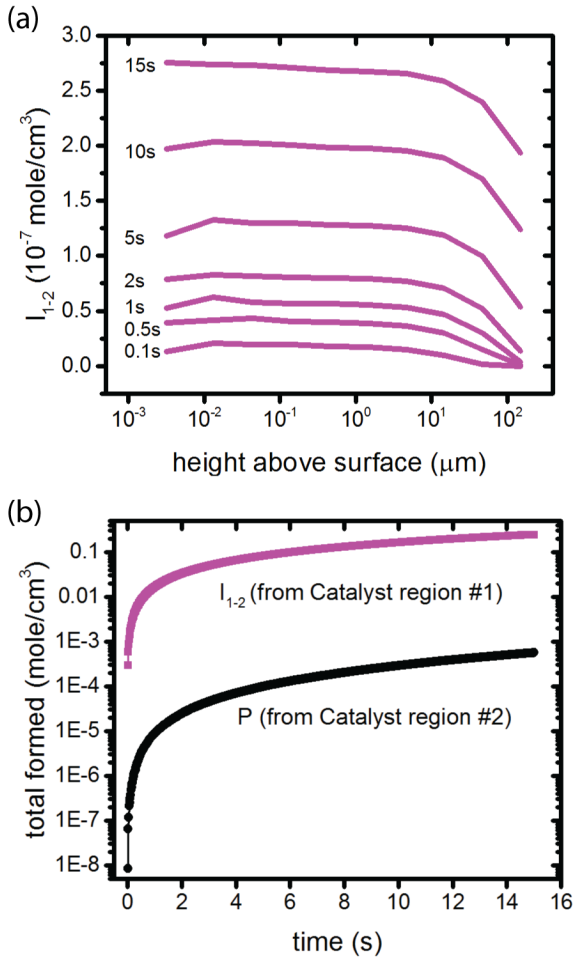

Figure 8. Functioning of a 2-site catalytic cascade where sites are adjacent and have matched kinetics. (a) distribution of $I_{1\text{-}2}$ in the electrolyte as a function of time (the reactant concentration is 3 x 10^{-4} moles/cm^3); (b) production of $I_{1\text{-}2}$ by catalytic region #1 and *P* by catalytic region #2.

These simple simulations provide some initial information towards design rules for artificial cascades: proximity and rate matching of a sequence of sites does not guarantee that a

cascade will be efficient because diffusion is not sufficiently constrained. A mechanism that can direct intermediates between 2 sites is clearly advantageous. Importantly, as discussed earlier in this section, much more information is needed than energetics to tailor catalytic rates to function well in a cascade, and as discussed in the Introduction, to reach efficiency and selectivity targets using time-varying solar illumination as the sole source of energy. Our understanding of what information is needed, and how to use it, is primitive for cascaded reactions in artificial photosynthetic systems. Natural systems, on the other hand, provide important lessons to inspire architectures that may have improved function and enable a connection to be made between catalyst selection and useful system designs.

Nature-inspired design rules

Plants need to deal with the fluctuation of light intensity and temperature within the day and during the year in the dynamically changing environment. Such seasonal and diurnal variation is somewhat systematic, but the changes also occur irregularly due to weather and canopy. Plants must adjust their photosynthetic performance to these unpredictable and constantly changing environments. They use multiple hierarchical strategies to control and adapt to maintain their performance, which arises from the structural and architectural flexibilities and the information flow network embedded in the system. Such a complicated control mechanism has not been incorporated into the design of artificial photosynthesis. In particular, we have not yet explored dynamic components to enhance system performance and durability in use. Design concepts analogous to those found in plants will likely become feasible with the advancement of material sciences and computational capabilities. In this section we describe some of the key elements of

natural systems that reveal how to deliver and use an information signal to enable the system to respond to its new environment within its timescale. Information flow in response to dynamically changing energy landscape may involve using the concentration gradients of ions, electrostatic effects, and so on.

Below we discuss three different level of control mechanisms that photosynthetic systems have to optimize performance in sunlight: (i) the atomic-scale control of the multielectron/proton catalytic reaction, with the water oxidation reaction in PSII as an example, (ii) electron flow between enzymes in thylakoid membranes, and (iii) chloroplast movement in the cell level. We note that this section does not cover all the design strategies that oxygenic photosynthesis systems have, but we touch on some strategies that plants have developed over their evolutionary timescale to adapt to dynamically changing environments.

Sequential multielectron/multiproton reactions at molecular level. Natural enzymes do complicated catalysis that involves multielectron/multiproton reactions. Nature uses remarkably varied systems and mechanisms to perform complex chemical transformations with efficiency, speed, and specificity. At the active site of many enzymes are metal centers, responsible for the rearrangement of electrons, protons, and atoms to carry out electron transfer and catalytic reactions. Such reactions include water oxidation with PSII,[75,76] CO_2 reduction with formate dehydrogenase and carbonic anhydrase,[77–79] hydrogen evolution with hydrogenase,[80] and nitrogen fixation with nitrogenase.[81–83] These reactions are carried out under ambient conditions and in a highly controlled manner, in both time and space, by utilizing the flexibility of the protein

environment, and the multiplicity of transition metal *d*-orbitals. For the past decades, there have been a tremendous effort to learn from natural systems and create structurally similar catalytic centers.[84,85] However, this strategy does not work for creating the desired functionality in many cases. More recently, the important role of the 2nd coordination sphere has been emphasized.[86,87] Furthermore, the effect of the reaction environment has also been recognized and discussed more in the recent studies.[88–90]

Here we use the recent studies of the water oxidation reaction in PSII as an example, to look at the role of the protein/hydrogen bond network.[91,92] Owing to the advancement of room temperature crystallography at X-ray free electron laser facilities, one can visualize the dynamically changing reaction environment of PSII during the water oxidation reaction.[91,93] In PSII, light-driven oxidation of water to molecular oxygen is catalyzed by the oxygen-evolving complex (OEC), consisting of a Mn_4CaO_5 cluster. This multi-electron, multi-proton catalysis requires the transport of two water molecules to and four electrons and four protons from the OEC (**Figure 9(a)**).[91,94]

Among the several hydrophylic pathways that extend from the OEC to bulk (**Figure 9(b)**), it has been proposed that the O1 channel is used for bringing substrate water in to the OEC, and the Cl1 channel is used for a proton release from the OEC to luminal side of the thylakoid membranes during the S_2 to S_3 transition. In particular, the release of a proton from the OEC seems to be highly controlled, and the narrow bottleneck region (**Figure 9(b)** inset), formed by the amino acid residues in the Cl1 channel, likely plays a role in regulating such flow.[93] The open and closed state of the proton gate appears to be controlled by the long-range electrostatic

effect originated from the redox changes at the OEC. The hydrogen-bonding network formed by the amino acid residues and water molecules create an efficient path to transfer information.

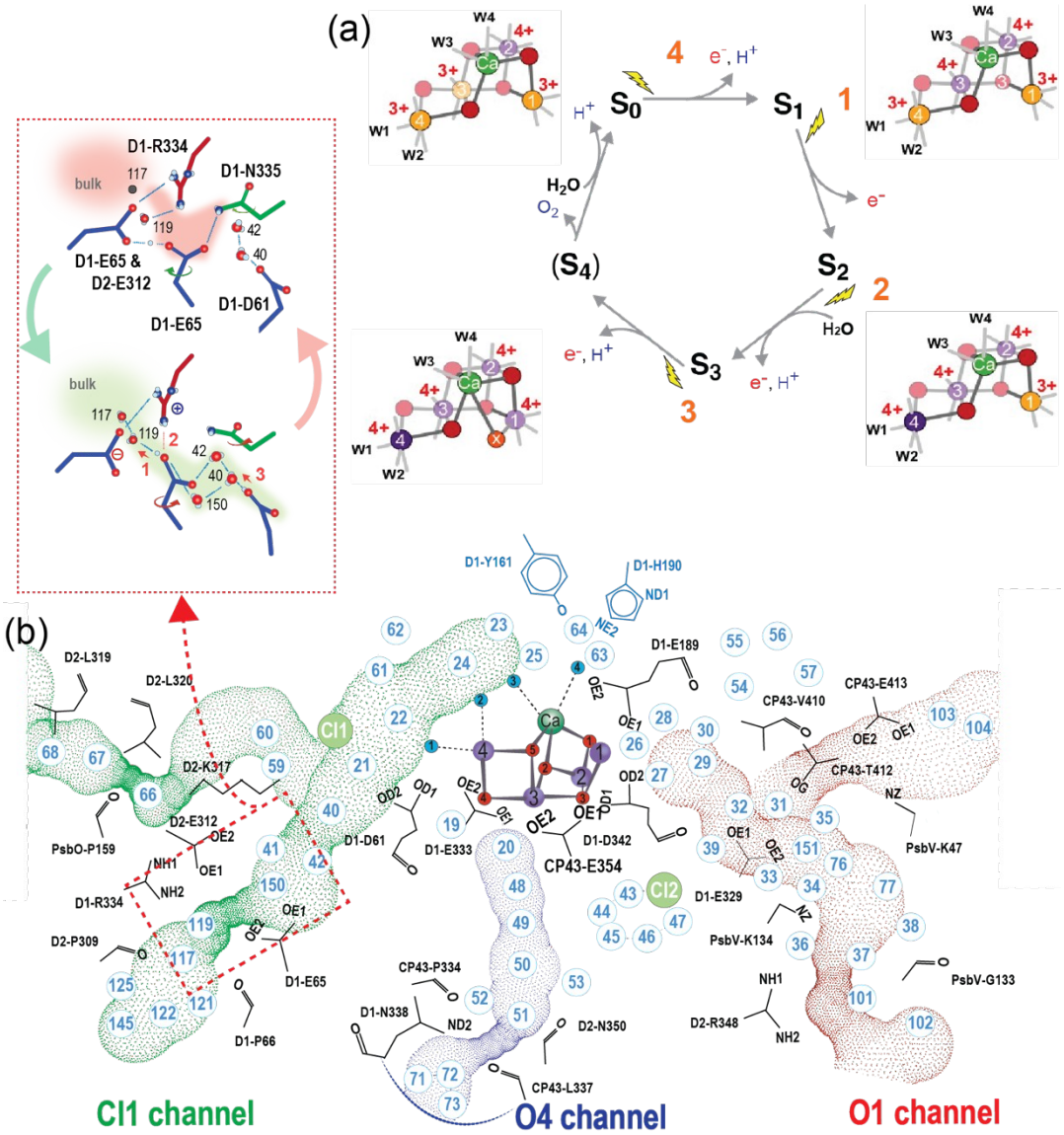

Figure 9. (a) Kok cycle of the water oxidation reaction in PSII. The structural models of the stable intermediates (S_0 to S_3) from the crystallography studies are shown. (b) Several hydrophilic channels extended from the OEC to bulk. In one of the S-state transitions (S_2 to S_3) during the water oxidation reaction, the O1 channel has been proposed as a water intake channel, and the Cl1 channel as a proton release channel. In the Cl1 channel, the bottleneck region (see the inset) shows reversible structural changes. This area likely functions as a proton gate. Adapted with permission from Refs 91 and 94. Copyright 2018, Springer Nature Limited. Copyright 2020, The Authors. Published by the Proceedings of the National Academy of Sciences.

Electron transfer in the thylakoid membranes. Regulating electron transport is important in artificial photosynthesis, as excess electrons promote unwanted redox reactions, and lead to the failure of the system. Controlling electron flow is also critical in natural photosynthesis to maintain its performance. In oxygenic photosynthesis, absorption of solar photons initiates electron transfer in the thylakoid membranes through two reaction centers, Photosystem I (PSI) and PSII, which leads to the synthesis of NADPH and ATP via linear electron transport (LET) (**Figure 10**).[95] The reducing power of NADPH and the chemical energy of ATP are then used to drive the Calvin cycle for CO_2 reduction and biosynthesis. In the process, the production of NADPH and ATP need to balance with the later metabolic demand of the organisms, in order for the organisms to adapt to their environmental conditions. To regulate the stoichiometry of ATP/ NADPH,[96] an additional electron transport pathway exists that recycles electrons around PSI, called cyclic electron transport (CET) (**Figure 10**).[97] Unlike LET, CET is driven only by PSI, through the redirection of the electron flow from ferredoxin (Fd) to plastoquinone (PQ). This results in only the production of ATP without net NADPH synthesis, thus increasing the ATP/NADPH ratio. Through the combination of LET and CET, natural photosynthesis regulates the electron transport.[98] Redirecting electron transport as a strategy to regulate the number of electrons at (photo)electrode that contributes to redox reactions, and scavenge them, if necessary, may be a valid strategy to incorporate into artificial photosynthetic designs.

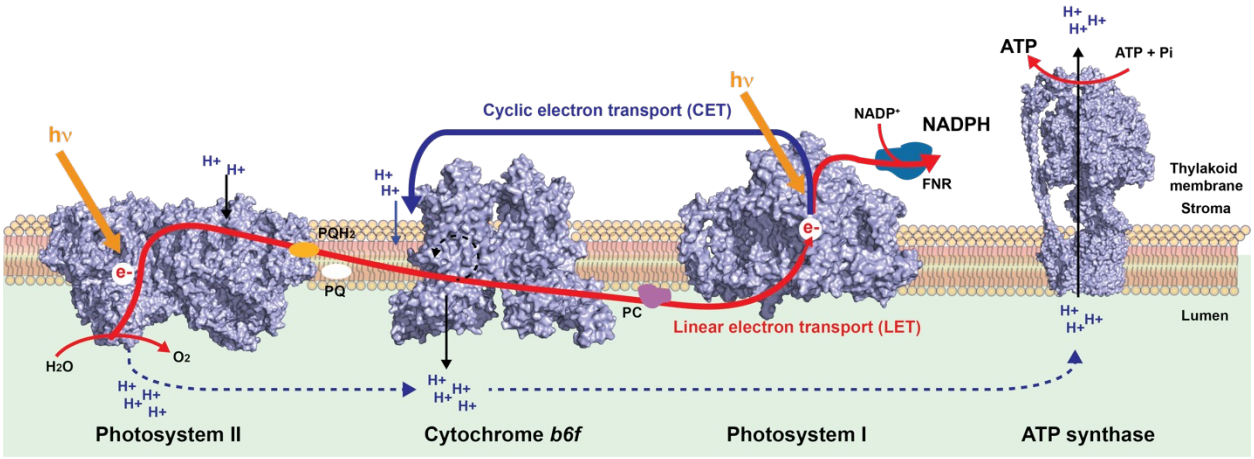

Figure 10: Linear (LET) and cyclic electron transport (CET) in photosynthetic systems. The photochemical water oxidation in PSII generates electrons, which transfer through plastoquinone (PQ), cytochrome (Cyt) b6f, and plastocyanin (Pc). PSI further transports electron from Pc to ferredoxin (Fd), which provides the electron to ferredoxin-$NADP^+$ reductase (FNR) to generate NADPH. The protons accumulated in the lumen during the process is used by ATP synthase to drive ATP synthesis. Adapted with permission from Ref 95. Copyright 2012, The Author. Published by Blackwell Publishing Limited.

Chloroplast movement in plant cells to regulate light absorption. Plants and algae cells contain a compartment (organelle) called a chloroplast, that contains photosynthetic enzymes.[99–101] The relocation of chloroplasts in the cell is used to control absorbing light intensity to avoid photodamage, and this is done by adjusting the orientation of thylakoid membranes in the cells relative to the incident light direction. **Figure 11** shows examples of the movement of plant organelles due to the light intensity. If the thylakoid membranes are oriented parallel to the incident light, less light is absorbed and therefore the cell can avoid excess absorption of solar radiation under high light conditions (**Figure 11(a)**). On the other hand, if the membranes are oriented perpendicular, more light is absorbed. This orientation is beneficial to enhance light absorption under low light conditions (**Figure 11(a)**).[99] The reorganization of chloroplasts is

known to occur with a speed of ≤ 2 mm/min. In the plant cells, the photoreceptor proteins (called phototrophins) sense light intensity and modify the polymer network (called actin) that is attached to the chloroplast. This initiates the reorientation of chloroplasts along the inner membrane of the cell (cytoplasm).

Going from the cell level to the membrane level (**Figure 11(b)**), thylakoid membranes in the chloroplast also react with light to change their morphology to regulate photosynthetic reactions.[101,102] PSII is located in the grana stacks, while PSI and ATP synthase are located in the stromal lamellae. Cytb6f is present in both domains. Thus, the morphological changes of thylakoid membranes affect electron transport. When the thylakoid membranes see light, the thylakoid lumen becomes swollen due to osmotic water fluxes. This allows mobility of the electron carrier (plastocyanin) in the lumen, and increases the electron transport rate between the two reaction centers, PSI and PSII.[103–105] Under excess light conditions, another photoprotection mechanism is activated, to dissipate excess energy into heat, and to decrease the antenna size so that PSII absorbs less photon energy. This is also accompanied by the re-distribution of proteins in the membrane. When the system cannot handle excess energy, photooxidative damage occurs in PSII, in which a part of the damaged protein (the D1 subunit) needs to be replaced (repair mechanism). In sum, plants manipulate the morphology of the confined space formed by membranes, to dynamically regulate electron flux, proton gradients, and chemical processes.

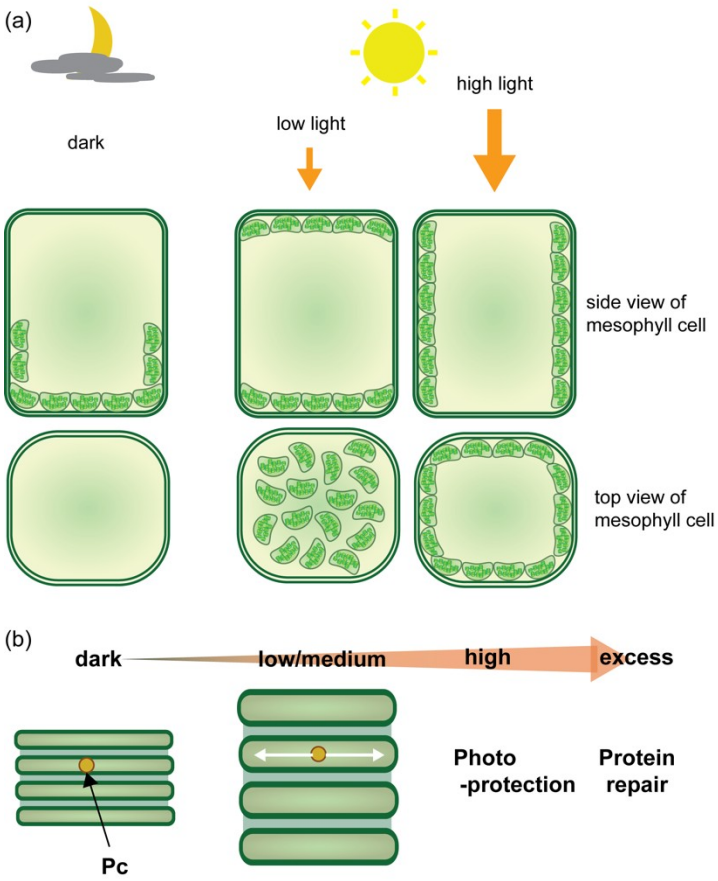

Figure 11: (a) Chloroplast movement in mesophyll cells. Depending on the light intensity, chloroplasts change its location so that the incident sunlight exposure of the thylakoid membranes system increased (low light) or decreased (high light). (b) Changes of thylakoid membrane swelling due to the light intensity. Adapted with permission from Refs 100 and 101. Copyright 2019, The Author. Published by the New Phytologist Trust. Copyright 2018, The Company of Biologists Ltd.

From nature to artificial systems

The sophisticated multi-level architectures of living photosynthetic systems enables sequences of chemical reactions to be selective and as efficient as possible, and additionally offer multiple durability mechanisms through self-protection and self-repair in sunlight. They present an important inspiration for ways to enable artificial systems to have high selectivity and good efficiency under diurnal conditions by providing a path for their catalytic cascades to be improved. We propose that by going beyond implementations of the thylakoid membrane's Z-scheme for conversion of light energy into stored chemical energy, artificial systems will benefit from component designs that utilize flexible structures such as those of proteins, or structures that accumulate charges like oxo complexes do as catalytic centers.

In the preceding section, we saw that natural systems organize the photoexcitations and chemistry in space and time in order to assure efficiency, and use electrons, ions and molecules as information to connect system elements and manage the broad span in timings involved in the photosynthetic process. Using this information as signals, the natural system can adapt dynamically to external conditions and optimize its efficiency. Signaling takes place via the environment of the central structure, whether a protein or an organelle, primarily by photoexcitations. These lead to morphological and structural changes that influence the transfer of electrons and chemical species. These changes can include variations in molecular conformations to control light absorption, and widening or narrowing diffusion pathways. From

a chemical kinetics perspective, signaling means dynamic control of the rate of a reaction by a change in populations or a change in rate coefficients, or both. Signaling mechanisms have evolved to protect the life of the plant by ensuring it can continuously produce sugars efficiently and heal damaged elements. Artificial photosynthetic systems, while not living, have basically the same requirements. Bio-inspired structures have been explored with the assumption that function will follow form,[85,106] and have not yet proven to be significantly superior to natural photosynthesis in overall solar energy conversion efficiency.[107] It is worth considering whether the opposite approach of focusing entirely on bio-inspired function to manage the overall photo-driven chemical conversion process could provide a means of improving artificial systems especially for CO_2 reduction.

In this section, we bridge from our examination of how to evaluate catalytic reaction rates, which are central, and discuss how to use inverse design to make better use of our knowledge of natural systems to design artificial ones that avoid bottlenecks (hurry up and wait) in the overall process that converts reactants into products. An optimum artificial system has to be able to completely convert every CO_2 molecule that it takes up into a specific desired product. What would a system that does this by mimicking natural function, taking advantage of information and signaling - and therefore is maximally efficient - look like?

System design criteria. As discussed in the Introduction in the context of inverse design a cascade of catalysts should be rate matched so that no catalyst in the sequence is idle. Overall catalytic rates cannot be assessed by consideration of energetics alone, there must be in-depth

knowledge of the catalytic reaction mechanisms in the system environment: a system of reaction steps at each catalyst will have complex responses to changes in populations and to energetics due to catalyst remodeling, adsorbate interactions and so on which must be taken into account. No matter how carefully matched, the inevitable timing stochastics of reaction steps at individual catalytic centers requires a buffering mechanism to store intermediates or reactants until needed, at which point they must be delivered efficiently. Effective rate matching requires that each catalyst operates at a higher turnover frequency than the one preceding it so that there is a concentration gradient to direct diffusion of intermediates from catalyst to catalyst. Ideally, transfer of intermediates along the cascade would be done through a confining channel to avoid their dilution, which places requirements on spatial arrangements of catalytic centers. The variability in rates due to variations in the solar resource through the day must also be accommodated. To do so, all the catalysts should have the same rate trends with photovoltages and photocurrents. All of these functions can potentially be enabled by signaling and transfer of information throughout the system. **Table 5** summarizes some proposed processes, and details are discussed below.

Table 5. Signaling and information transfer for efficient CO_2 reduction

Information type	**Signal**	**Function**
Photoexcitations to generate electrons, protons or molecules	Transient change in populations at the system level	Balance photodriven and non-photodriven processes
Time-dependent currents into and out of catalytic regions	Change in local populations of electrons and protons	Balance rates of reduction and oxidation reactions
Reaction rates	Concentration fluctuations	Using confinement to optimize overall system efficiency

Signaling via photoexcitation. Chloroplast movement via swelling and deswelling controls the amount of light absorbed by antennas, then used by PSI and PSII. This function can be performed artificially by incorporating system elements that can be switched between states that do and do not transmit visible light via specific photoexcitations that induce dynamical changes in their conformations and hence their absorptivity. An example is azobenzene, which is a versatile and robust fast-switching molecule triggered by UV and visible light.[108] It has been incorporated into polymers to drive photo-mechanical changes[109,110] and for reversible light attenuation.[111] Thiophene-substituted fluorinated cyclopentenes have also been evaluated as photoswitchable components of photoresist systems for nanopatterning.[112] Such switching elements have not been incorporated into artificial photosynthetic systems to our knowledge, but could be added as coatings on transparent supports, or as liquids in between plates. They could be driven by an auxiliary UV light source such as a light-emitting diode is incorporated into the system powered by an embedded photovoltaic and associated electronics. This function would use light to provide dynamic control over reactivity beyond the central photoelectrochemical processes, and would potentially be activated by accumulation of charge with an accompanying change in voltage.

Signaling by electron and proton transport. It has been recognized for some time that a reduced energy pathway for transfer of electrons and protons over any distance can be realized if both are transferred together, PCET. This process has been extensively studied in biological and

non-biological systems. PCET can be unidirectional, meaning that electrons and protons are transferred between the same two locations. In this case, transfer can be simultaneous, or stepwise albeit with the two steps very close together in time, a situation very difficult to distinguish from simultaneous transfer.[113,114] It has been proposed in a theoretical study that more than one electron can be passed at a time if that path is the lowest energy one.[115]

Molecular arrangements surrounding the source and destination of PCET significantly affect the process, with local water structure being of particular importance.[116] PCET can also be bidirectional and asynchronous, with electrons and protons taking different pathways.[117] How asynchronous PCET is manifested in non-biological electrochemical systems where the overall reaction requires transfer of multiple protons and electrons has also been examined.[118] Placement of the reactive centers involved in PCET next to each other is a clear strategy to implement the process in artificial systems. However, if this is not possible or desirable, more complex transfer pathways need to be provided. One possibility is to embed the centers that undergo PCET into structures like ionized porous polyelectrolyte frameworks, which provide an interesting environment that can promote enhanced transport and reactivity. They enable electrostatic interactions in addition to size-sieving, and provide mobility for free charges in photochemical and electrochemical applications.[119] These materials have not been used in artificial photosynthetic systems, but could prove a useful starting point for improved architectures as they offer the potential for independent control of proton transfer (proton motive force) and electron transfer.[85] It is also possible that a CET-like chemical process could be used in solution for independent control of electron and proton concentrations. A process that enables electron recirculation to occur independent of the cathode has been identified using reaction-diffusion

simulations of the electrolyte chemistry in porous photoanodes used for dye-sensitized solar cells.[120] The mechanism involves pushing the electrolyte reactions within the pore far from equilibrium during the solar photon to electron conversion process, thus providing a kinetically important route for electrolyte redox reactions to occur in these confined spaces. Extension of this phenomenon to systems involving both electrons and protons provides an additional possible architecture.

Signaling by accumulation of reagents. As noted previously, the inherent stochasticity of reaction steps at individual catalytic centers limits our ability to closely synchronize a specific pair of sites. Provision of buffering elements where reagents (electrons, protons and molecular intermediates) can be stored temporarily would provide a very useful way to avoid idle catalytic centers, and improve efficiency. Natural systems such as PSII do this by including channels that can control the flow of protons and water,[121] and have mechanisms to dissipate excess electrons through cyclic electron transport.[97] Accumulation of photogenerated electrons[122] and holes[123] in oxide semiconductors has been reported, with the caveat that an increase in their concentration may increase losses through recombination. Cross-surface electron transfer to accumulate redox equivalents in molecular catalyst-dye mixtures has been proposed.[124] A polyoxometallate structure that stores electrons and uses them for hydrogen formation when there is no light has been described.[125] Accumulation of water and protons can occur in polyelectrolytes such as Nafion,[126] however mechanisms that use this accumulation as information to enable their release are not clear. Storage of molecular substrates via provision of nanocavities in copper CO_2 reduction catalysts that increase their residence time and promote C-C coupling reactions is also

possible.[127] This strategy could be very useful if mechanisms for stabilizing the copper nanoscale morphology, which is very labile during catalysis,[128,129] are found. It is clear that building in reservoirs would add an important level of control and coordination to artificial systems, however how to do this in an intentional and general way requires new science.

Confinement and compartmentalization to promote signaling. Chloroplasts are highly organized structures, containing closed compartments with free space in between, and membranes covering large surface areas, with each component present playing an important role in the natural photosynthetic process. Confinement ensures that key reactants are close to each other, and that creation and consumption of just a few of them will lead to large local concentration changes, and therefore large changes in reaction rates. There are a number of examples for how compartmentalization can be used in artificial systems, however there is much room for new concepts. Biomimetic structures such as liposome scaffolds have been investigated, with potential uses for tandem catalysis.[130] It was recognized that placement of molecular components into these scaffolds must be done with care to control electron exchange between them. Organic polyelectrolyte films have long been used as separators to isolate anodic from cathodic reactions, and as supports for catalysts in membrane-electrode assemblies. Accordingly, key properties they must have to function well in systems are identified.[131–133] These membrane films are on a completely different thickness scale than those in a chloroplast, however, so function beyond physical separation and support, such as channeling of redox mediators, may not be readily accessible. Moreover, organic polymer membrane permeability to neutral species such as CO_2 and O_2 and their reaction products can be significant, leading to these

species being present throughout the artificial system, whether wanted or not, and permeability can vary with time.[134,135] Whether or not useful isolation of regions can be achieved with artificial membrane walls, molecular catalysts can be embedded in metal-organic and covalent organic frameworks to provide them with beneficial local environments,[19,136] and catalytic electrodes can be coated with electrodeposited organic layers that promote C-C bond formation.[137,138] Development of these strategies along with compartmentalization approaches using porous inorganic materials[139] to mimic natural function could enable new artificial architecture concepts that promote efficient light-driven catalytic cascades. Catalysts can also be coated with electrodeposited layers that could also promote cooperative effects by inter-catalyst communication through exchange of information (electrons, holes, protons, molecules) in a manner analogous to allostery.[140] Even if such a sophisticated outcome is not easily attained, at least such structures would promote substrate channeling, which is not routinely implemented in artificial systems although it is ubiquitous in natural ones[141] and whose study has led to useful design principles applicable to synthetic biological systems.[142,143]

Summary and outlook

As artificial photosynthetic systems have evolved from early implementations for water splitting and H_2 generation - based on the Z-scheme that converts light energy into chemical energy - to photoelectrochemical conversion of CO_2 into complex products, it has become clear that the Z-scheme alone is not sufficient to ensure high efficiency and selectivity for chemical reactions that require more than two photons to form a desired product. Using a combination of inverse and forward design processes, we have considered how to reach a performance target for

CO_2 reduction transformations that are both selective and efficient, connecting what we know how to do today to what is needed to reach this target. We take as a fundamental principle that at least two separate catalytic centers organized in a cascade are required in artificial systems, and discuss how to use biology to progress beyond what is known today about artificial systems based on heterogeneous catalysis to new systems capable of reaching this performance target.

The sequence of steps in natural photosynthetic processes that use water and sunlight to convert CO_2 into useful chemicals is lengthy, but optimized through evolution to be as energetically and atom-efficient as possible. These steps involve reduction, oxidation, bond breaking and making, and transport. Each has its own characteristic timing, depending on its instantaneous rate, which constrains how well the steps can be coupled so that the entire system is active when the sun shines on it. Important mechanisms such as internal signaling, substrate channeling, reactant accumulation and light control mediate this coupling, to the plant's advantage. Bioinspired structures to reproduce catalytic centers and their immediate environment as well as bioinspired functions out to the second coordination sphere of the catalyst are being explored, however we argue that there are highly compelling opportunities if the function of the entire biological system is the starting point. To form a multicarbon product from CO_2 selectively and with the maximum efficiency, each catalyst in a cascade must be specifically selected to be highly active at the system's photovoltage. This cannot be done by simply inspecting the energetics of the reaction path, the full kinetics of the system must be used to understand what controls its rate and how competing reactions might affect the catalyst's reactivity. When multiple catalytic centers are assembled in a sequence connected by transfer paths, their reactivity as a system can be assessed. This is not sufficient to ensure that the target

of good overall selectivity and efficiency can be reached, however, additional elements are needed.

To approach the specificity of natural systems, we examine which of their characteristics will provide advantages for artificial constructs. We identify the importance of tailoring the catalysts' environments to optimize their reactivity as well as a buffer zone for storage of reactants until needed, and the advantage of providing pathways for directed transport between the catalytic centers. We include the possibility of active light regulation as a means of controlling overall rates in these multistep processes. These functions alone are likely not enough to provide system-level coordination, however. We discuss how a more global function of the natural systems, signaling and information flow, might provide a means for superior performance of artificial systems, but intentionally providing system components that are receptive to changes in stimuli, and drive beneficial responses. Changes in concentrations and fluxes of photons, electrons, protons and molecules have the potential to serve as signaling agents, and learning how to use them will advance not only artificial photosynthetic science and technology to reach the high performance level that has been targeted, but also our understanding of how natural systems work.

Associated Content

Supporting Information. Details of the simulations and their results are available free of charge from Zenodo at DOI:10.5281/zenodo.7555776.

Author Information

Author Contributions

The manuscript was written through contributions of all authors. Conceptualization: FAH. Formal Analysis, Validation: JWA and FAH. Investigation, Funding acquisition, Visualization, Writing: JY, JWA, FAH.

Notes

The authors declare no competing financial interests.

Funding

This material is based upon work performed by the Liquid Sunlight Alliance, which is supported by the U.S. Department of Energy, Office of Science, Office of Basic Energy Sciences, Fuels from Sunlight Hub under Award Number DE-SC0021266 (FAH, kinetics of single and cascaded catalytic systems, artificial signaling) and by the Clean Energy Manufacturing Program, U.S. Department of Energy, Office of Science, Office of Basic Energy Sciences, Chemical Sciences, Geosciences, and Biosciences Division, in under Contract No. DE-AC02-05CH11231 (JY and JWA, degree of rate control and biomimetic signaling functions).

Acknowledgements

We are grateful to Dr. William Hinsberg (Columbia Hill Technical Consulting), Ms. Chenqi Fan (LBNL and UC Berkeley) and Drs Frank Abild-Pedersen and Michael Tang (SLAC National Accelerator Laboratory) for their contributions to construction of the interfacial kinetics models and helpful discussions and suggestions.

References

(1) Calvin, M. Artificial Photosynthesis: Quantum Capture and Energy Storage. *Photochem Photobiol* **1983**, *37* (3), 349–360. https://doi.org/10.1111/j.1751-1097.1983.tb04484.x.

(2) Gerischer, H. Heterogeneous Electrochemical Systems for Solar Energy Conversion. *Pure and Applied Chemistry* **1980**, *52* (12), 2649–2667. https://doi.org/10.1351/pac198052122649.

(3) Niu, F.; Wang, D.; Li, F.; Liu, Y.; Shen, S.; Meyer, T. J. Hybrid Photoelectrochemical Water Splitting Systems: From Interface Design to System Assembly. *Adv. Energy Mater.* **2020**, *10* (11), 1900399. https://doi.org/10.1002/aenm.201900399.

(4) Goto, Y.; Hisatomi, T.; Wang, Q.; Higashi, T.; Ishikiriyama, K.; Maeda, T.; Sakata, Y.; Okunaka, S.; Tokudome, H.; Katayama, M.; Akiyama, S.; Nishiyama, H.; Inoue, Y.; Takewaki, T.; Setoyama, T.; Minegishi, T.; Takata, T.; Yamada, T.; Domen, K. A Particulate Photocatalyst Water-Splitting Panel for Large-Scale Solar Hydrogen Generation. *Joule* **2018**, *2* (3), 509–520. https://doi.org/10.1016/j.joule.2017.12.009.

(5) Fabian, D. M.; Hu, S.; Singh, N.; Houle, F. A.; Hisatomi, T.; Domen, K.; Osterloh, F. E.; Ardo, S. Particle Suspension Reactors and Materials for Solar-Driven Water Splitting. *Energy Environ. Sci.* **2015**, *8* (10), 2825–2850. https://doi.org/10.1039/C5EE01434D.

(6) Teodor, A. H.; Bruce, B. D. Putting Photosystem I to Work: Truly Green Energy. *Trends in Biotechnology* **2020**, *38* (12), 1329–1342. https://doi.org/10.1016/j.tibtech.2020.04.004.

(7) Zhang, J. Z.; Reisner, E. Advancing Photosystem II Photoelectrochemistry for Semi-Artificial Photosynthesis. *Nat Rev Chem* **2019**, *4* (1), 6–21. https://doi.org/10.1038/s41570-019-0149-4.

(8) Boutin, E.; Robert, M. Molecular Electrochemical Reduction of CO2 beyond Two Electrons. *Trends in Chemistry* **2021**, *3* (5), 359–372. https://doi.org/10.1016/j.trechm.2021.02.003.

(9) Nitopi, S.; Bertheussen, E.; Scott, S. B.; Liu, X.; Engstfeld, A. K.; Horch, S.; Seger, B.; Stephens, I. E. L.; Chan, K.; Hahn, C.; Nørskov, J. K.; Jaramillo, T. F.; Chorkendorff, I. Progress and Perspectives of Electrochemical CO_2 Reduction on Copper in Aqueous Electrolyte. *Chem. Rev.* **2019**, *119* (12), 7610–7672. https://doi.org/10.1021/acs.chemrev.8b00705.

(10) Chen, C.; Li, Y.; Yu, S.; Louisia, S.; Jin, J.; Li, M.; Ross, M. B.; Yang, P. Cu-Ag Tandem Catalysts for High-Rate CO2 Electrolysis toward Multicarbons. *Joule* **2020**, *4* (8), 1688–1699. https://doi.org/10.1016/j.joule.2020.07.009.

(11) Guo, S.; Asset, T.; Atanassov, P. Catalytic Hybrid Electrocatalytic/Biocatalytic Cascades for Carbon Dioxide Reduction and Valorization. *ACS Catal.* **2021**, *11* (9), 5172–5188. https://doi.org/10.1021/acscatal.0c04862.

(12) Kong, C. J.; Warren, E. L.; Greenaway, A. L.; Prabhakar, R. R.; Tamboli, A. C.; Ager, J. W. Design Principles of Tandem Cascade Photoelectrochemical Devices. *Sustainable Energy Fuels* **2021**, *5* (24), 6361–6371. https://doi.org/10.1039/D1SE01322J.

(13) Meng, D.; Zhang, M.; Si, D.; Mao, M.; Hou, Y.; Huang, Y.; Cao, R. Highly Selective Tandem Electroreduction of CO_2 to Ethylene over Atomically Isolated Nickel–Nitrogen Site/Copper Nanoparticle Catalysts. *Angew Chem Int Ed* **2021**, *60* (48), 25485–25492. https://doi.org/10.1002/anie.202111136.

(14) Lin, L.; Liu, T.; Xiao, J.; Li, H.; Wei, P.; Gao, D.; Nan, B.; Si, R.; Wang, G.; Bao, X. Enhancing CO_2 Electroreduction to Methane with a Cobalt Phthalocyanine and Zinc–Nitrogen–Carbon Tandem Catalyst. *Angew Chem Int Ed* **2020**, *59* (50), 22408–22413. https://doi.org/10.1002/anie.202009191.

(15) She, X.; Zhang, T.; Li, Z.; Li, H.; Xu, H.; Wu, J. Tandem Electrodes for Carbon Dioxide Reduction into C2+ Products at Simultaneously High Production Efficiency and Rate. *Cell Reports Physical Science* **2020**, *1* (4), 100051. https://doi.org/10.1016/j.xcrp.2020.100051.

(16) Kuk, S. K.; Singh, R. K.; Nam, D. H.; Singh, R.; Lee, J.-K.; Park, C. B. Photoelectrochemical Reduction of Carbon Dioxide to Methanol through a Highly Efficient Enzyme Cascade. *Angew. Chem. Int. Ed.* **2017**, *56* (14), 3827–3832. https://doi.org/10.1002/anie.201611379.

(17) Lum, Y.; Ager, J. W. Sequential Catalysis Controls Selectivity in Electrochemical CO_2 Reduction on Cu. *Energy Environ. Sci.* **2018**, *11* (10), 2935–2944. https://doi.org/10.1039/C8EE01501E.

(18) Zhang, X.-P.; Chandra, A.; Lee, Y.-M.; Cao, R.; Ray, K.; Nam, W. Transition Metal-Mediated O–O Bond Formation and Activation in Chemistry and Biology. *Chem. Soc. Rev.* **2021**, *50* (8), 4804–4811. https://doi.org/10.1039/D0CS01456G.

(19) Proppe, A. H.; Li, Y. C.; Aspuru-Guzik, A.; Berlinguette, C. P.; Chang, C. J.; Cogdell, R.; Doyle, A. G.; Flick, J.; Gabor, N. M.; van Grondelle, R.; Hammes-Schiffer, S.; Jaffer, S. A.; Kelley, S. O.; Leclerc, M.; Leo, K.; Mallouk, T. E.; Narang, P.; Schlau-Cohen, G. S.; Scholes, G. D.; Vojvodic, A.; Yam, V. W.-W.; Yang, J. Y.; Sargent, E. H. Bioinspiration in Light Harvesting and Catalysis. *Nat Rev Mater* **2020**, *5* (11), 828–846. https://doi.org/10.1038/s41578-020-0222-0.

(20) Wagner, A.; Sahm, C. D.; Reisner, E. Towards Molecular Understanding of Local Chemical Environment Effects in Electro- and Photocatalytic CO2 Reduction. *Nat Catal* **2020**, *3* (10), 775–786. https://doi.org/10.1038/s41929-020-00512-x.

(21) Kondo, M.; Tatewaki, H.; Masaoka, S. Design of Molecular Water Oxidation Catalysts with Earth-Abundant Metal Ions. *Chem. Soc. Rev.* **2021**, *50* (12), 6790–6831. https://doi.org/10.1039/D0CS01442G.

(22) Colburn, S.; Majumdar, A. Inverse Design and Flexible Parameterization of Meta-Optics Using Algorithmic Differentiation. *Commun Phys* **2021**, *4* (1), 65. https://doi.org/10.1038/s42005-021-00568-6.

(23) Massad, R.; Cheshire, T.; Fan, C.; Houle, F. Water Oxidation by a Dye-Catalyst Diad in Natural Sunlight: Timing and Coordination of Excitations and Reactions across Timescales of Picoseconds to Hours. *Chemical Science* **2023**, *14* (8), 1997–2008. https://doi.org/10.1039/D2SC06966K.

(24) Grela, M. A.; Coronel, M. E. J.; Colussi, A. J. Quantitative Spin-Trapping Studies of Weakly Illuminated Titanium Dioxide Sols. Implications for the Mechanism of Photocatalysis. *J. Phys. Chem.* **1996**, *100* (42), 16940–16946. https://doi.org/10.1021/jp953562r.

(25) Shon, M. J.; Cohen, A. E. Mass Action at the Single-Molecule Level. *J. Am. Chem. Soc.* **2012**, *134* (35), 14618–14623. https://doi.org/10.1021/ja3062425.

(26) Theaker, N.; Strain, J. M.; Kumar, B.; Brian, J. P.; Kumari, S.; Spurgeon, J. M. Heterogeneously Catalyzed Two-Step Cascade Electrochemical Reduction of CO2 to Ethanol. *Electrochimica Acta* **2018**, *274*, 1–8. https://doi.org/10.1016/j.electacta.2018.04.072.

(27) Gurudayal; Perone, D.; Malani, S.; Lum, Y.; Haussener, S.; Ager, J. W. Sequential Cascade Electrocatalytic Conversion of Carbon Dioxide to C–C Coupled Products. *ACS Appl. Energy Mater.* **2019**, *2* (6), 4551–4559. https://doi.org/10.1021/acsaem.9b00791.

(28) Gao, J.; Zhang, H.; Guo, X.; Luo, J.; Zakeeruddin, S. M.; Ren, D.; Grätzel, M. Selective C–C Coupling in Carbon Dioxide Electroreduction via Efficient Spillover of Intermediates As Supported by Operando Raman Spectroscopy. *J. Am. Chem. Soc.* **2019**, *141* (47), 18704–18714. https://doi.org/10.1021/jacs.9b07415.

(29) Cao, B.; Li, F.-Z.; Gu, J. Designing Cu-Based Tandem Catalysts for CO_2 Electroreduction Based on Mass Transport of CO Intermediate. *ACS Catal.* **2022**, *12* (15), 9735–9752. https://doi.org/10.1021/acscatal.2c02579.

(30) Zhang, Y.; Li, B.; Ma, S. Dual Functionalization of Porous Aromatic Frameworks as a New Platform for Heterogeneous Cascade Catalysis. *Chem. Commun.* **2014**, *50* (62), 8507. https://doi.org/10.1039/C4CC04012K.

(31) Gambo, Y.; Adamu, S.; Lucky, R. A.; Ba-Shammakh, M. S.; Hossain, M. M. Tandem Catalysis: A Sustainable Alternative for Direct Hydrogenation of CO2 to Light Olefins. *Applied Catalysis A: General* **2022**, *641*, 118658. https://doi.org/10.1016/j.apcata.2022.118658.

(32) Zhu, Y.; Cui, X.; Liu, H.; Guo, Z.; Dang, Y.; Fan, Z.; Zhang, Z.; Hu, W. Tandem Catalysis in Electrochemical CO2 Reduction Reaction. *Nano Res.* **2021**, *14* (12), 4471–4486. https://doi.org/10.1007/s12274-021-3448-2.

(33) Rayder, T. M.; Adillon, E. H.; Byers, J. A.; Tsung, C.-K. A Bioinspired Multicomponent Catalytic System for Converting Carbon Dioxide into Methanol Autocatalytically. *Chem* **2020**, *6* (7), 1742–1754. https://doi.org/10.1016/j.chempr.2020.04.008.

(34) Nørskov, J. K.; Abild-Pedersen, F.; Studt, F.; Bligaard, T. Density Functional Theory in Surface Chemistry and Catalysis. *Proc. Natl. Acad. Sci. U.S.A.* **2011**, *108* (3), 937–943. https://doi.org/10.1073/pnas.1006652108.

(35) Reuter, K. Ab Initio Thermodynamics and First-Principles Microkinetics for Surface Catalysis. *Catal Lett* **2016**, *146* (3), 541–563. https://doi.org/10.1007/s10562-015-1684-3.

(36) Ye, R.; Mao, X.; Sun, X.; Chen, P. Analogy between Enzyme and Nanoparticle Catalysis: A Single-Molecule Perspective. *ACS Catal.* **2019**, *9* (3), 1985–1992. https://doi.org/10.1021/acscatal.8b04926.

(37) Laidler, K. J. Rate Controlling Step: A Necessary or Useful Concept? *J. Chem. Educ.* **1988**, *65* (3), 250. https://doi.org/10.1021/ed065p250.

(38) Piccinin, S.; Stamatakis, M. CO Oxidation on Pd(111): A First-Principles-Based Kinetic Monte Carlo Study. *ACS Catal.* **2014**, *4* (7), 2143–2152. https://doi.org/10.1021/cs500377j.

(39) Stamatakis, M. Kinetic Modelling of Heterogeneous Catalytic Systems. *J. Phys.: Condens. Matter* **2015**, *27* (1), 013001. https://doi.org/10.1088/0953-8984/27/1/013001.

(40) Wiegel, A. A.; Liu, M. J.; Hinsberg, W. D.; Wilson, K. R.; Houle, F. A. Diffusive Confinement of Free Radical Intermediates in the OH Radical Oxidation of Semisolid

Aerosols. *Phys. Chem. Chem. Phys.* **2017**, *19* (9), 6814–6830. https://doi.org/10.1039/C7CP00696A.

(41) Razdan, N. K.; Lin, T. C.; Bhan, A. Concepts Relevant for the Kinetic Analysis of Reversible Reaction Systems. *Chem. Rev.* **2023**, acs.chemrev.2c00510. https://doi.org/10.1021/acs.chemrev.2c00510.

(42) Nørskov, J. K.; Studt, F.; Abild-Pedersen, F.; Bligaard, T. *Fundamental Concepts in Heterogeneous Catalysis*; pp36-39; Wiley: Hoboken, New Jersey, 2015.

(43) Righi, G.; Plescher, J.; Schmidt, F.-P.; Campen, R. K.; Fabris, S.; Knop-Gericke, A.; Schlögl, R.; Jones, T. E.; Teschner, D.; Piccinin, S. On the Origin of Multihole Oxygen Evolution in Haematite Photoanodes. *Nat Catal* **2022**, *5* (10), 888–899. https://doi.org/10.1038/s41929-022-00845-9.

(44) Corby, S.; Rao, R. R.; Steier, L.; Durrant, J. R. The Kinetics of Metal Oxide Photoanodes from Charge Generation to Catalysis. *Nat Rev Mater* **2021**, *6* (12), 1136–1155. https://doi.org/10.1038/s41578-021-00343-7.

(45) Wang, D.; Sheng, T.; Chen, J.; Wang, H.-F. F.; Hu, P. Identifying the Key Obstacle in Photocatalytic Oxygen Evolution on Rutile TiO2. *Nature Catalysis* **2018**, *1* (4), 291–299. https://doi.org/10.1038/s41929-018-0055-z.

(46) Campbell, C. T. Finding the Rate-Determining Step in a Mechanism. *Journal of Catalysis* **2001**, *204* (2), 520–524. https://doi.org/10.1006/jcat.2001.3396.

(47) Campbell, C. T. The Degree of Rate Control: A Powerful Tool for Catalysis Research. *ACS Catal.* **2017**, *7* (4), 2770–2779. https://doi.org/10.1021/acscatal.7b00115.

(48) Wang, B.; Chen, S.; Zhang, J.; Li, S.; Yang, B. Propagating DFT Uncertainty to Mechanism Determination, Degree of Rate Control, and Coverage Analysis: The Kinetics of Dry Reforming of Methane. *J. Phys. Chem. C* **2019**, *123* (50), 30389–30397. https://doi.org/10.1021/acs.jpcc.9b08755.

(49) Meskine, H.; Matera, S.; Scheffler, M.; Reuter, K.; Metiu, H. Examination of the Concept of Degree of Rate Control by First-Principles Kinetic Monte Carlo Simulations. *Surface Science* **2009**, *603* (10–12), 1724–1730. https://doi.org/10.1016/j.susc.2008.08.036.

(50) Avanesian, T.; Christopher, P. Scaled Degree of Rate Control: Identifying Elementary Steps That Control Differences in Performance of Transition-Metal Catalysts. *ACS Catal.* **2016**, *6* (8), 5268–5272. https://doi.org/10.1021/acscatal.6b01547.

(51) Deskins, N. A.; Dupuis, M. Intrinsic Hole Migration Rates in TiO_2 from Density Functional Theory. *J. Phys. Chem. C* **2009**, *113* (1), 346–358. https://doi.org/10.1021/jp802903c.

(52) Goodpaster, J. D.; Bell, A. T.; Head-Gordon, M. Identification of Possible Pathways for C–C Bond Formation during Electrochemical Reduction of CO 2 : New Theoretical Insights from an Improved Electrochemical Model. *The Journal of Physical Chemistry Letters* **2016**, *7* (8), 1471–1477. https://doi.org/10.1021/acs.jpclett.6b00358.

(53) Schouten, K. J. P.; Qin, Z.; Pérez Gallent, E.; Koper, M. T. M. Two Pathways for the Formation of Ethylene in CO Reduction on Single-Crystal Copper Electrodes. *J. Am. Chem. Soc.* **2012**, *134* (24), 9864–9867. https://doi.org/10.1021/ja302668n.

(54) Bunker, D. L.; Garrett, B.; Kleindienst, T.; Long, G. S. Discrete Simulation Methods in Combustion Kinetics. *Combustion and Flame* **1974**, *23* (3), 373–379. https://doi.org/10.1016/0010-2180(74)90120-5.

(55) Gillespie, D. T. A General Method for Numerically Simulating the Stochastic Time Evolution of Coupled Chemical Reactions. *Journal of Computational Physics* **1976**, *22* (4), 403–434. https://doi.org/10.1016/0021-9991(76)90041-3.

(56) Gillespie, D. T.; Hellander, A.; Petzold, L. R. Perspective: Stochastic Algorithms for Chemical Kinetics. *The Journal of Chemical Physics* **2013**, *138* (17), 170901. https://doi.org/10.1063/1.4801941.

(57) Hinsberg, William; Houle, Frances. Software Architecture for Stochastic Simulation of Non-Homogeneous Systems. US Patent No. 5826065, October 20, 1998.

(58) Gillespie, D. T. Stochastic Simulation of Chemical Kinetics. *Annu. Rev. Phys. Chem.* **2007**, *58* (1), 35–55. https://doi.org/10.1146/annurev.physchem.58.032806.104637.

(59) Hinsberg, William; Houle, Frances. Kinetiscope, Https://Www.Hinsberg.Net/Kinetiscope; Accessed August 24,2022.

(60) Hinsberg, William; Houle, Frances. Stochastic Simulation Method for Processes Containing Equilibrium Steps. US Patent No. 5625579, April 29, 1997.

(61) Hinsberg, William; Houle, Frances. Method for Stochastic and Deterministic Timebase Control in Stochastic Simulations. US Patent No. 5745385, April 28, 1997.

(62) Zijlstra, B.; Zhang, X.; Liu, J.-X.; Filot, I. A. W.; Zhou, Z.; Sun, S.; Hensen, E. J. M. First-Principles Microkinetics Simulations of Electrochemical Reduction of CO2 over Cu Catalysts. *Electrochimica Acta* **2020**, *335*, 135665. https://doi.org/10.1016/j.electacta.2020.135665.

(63) Liu, X.; Schlexer, P.; Xiao, J.; Ji, Y.; Wang, L.; Sandberg, R. B.; Tang, M.; Brown, K. S.; Peng, H.; Ringe, S.; Hahn, C.; Jaramillo, T. F.; Nørskov, J. K.; Chan, K. PH Effects on the Electrochemical Reduction of CO(2) towards C2 Products on Stepped Copper. *Nat Commun* **2019**, *10* (1), 32. https://doi.org/10.1038/s41467-018-07970-9.

(64) Schulz, K. G.; Riebesell, U.; Rost, B.; Thoms, S.; Zeebe, R. E. Determination of the Rate Constants for the Carbon Dioxide to Bicarbonate Inter-Conversion in PH-Buffered Seawater Systems. *Marine Chemistry* **2006**, *100* (1–2), 53–65. https://doi.org/10.1016/j.marchem.2005.11.001.

(65) Pocker, Y.; Bjorkquist, D. W. Stopped-Flow Studies of Carbon Dioxide Hydration and Bicarbonate Dehydration in Water and Water-D2. Acid-Base and Metal Ion Catalysis. *J. Am. Chem. Soc.* **1977**, *99* (20), 6537–6543. https://doi.org/10.1021/ja00462a012.

(66) Adamczyk, K.; Prémont-Schwarz, M.; Pines, D.; Pines, E.; Nibbering, E. T. J. Real-Time Observation of Carbonic Acid Formation in Aqueous Solution. *Science* **2009**, *326* (5960), 1690–1694. https://doi.org/10.1126/science.1180060.

(67) Wuttig, A.; Yoon, Y.; Ryu, J.; Surendranath, Y. Bicarbonate Is Not a General Acid in Au-Catalyzed CO_2 Electroreduction. *J. Am. Chem. Soc.* **2017**, *139* (47), 17109–17113. https://doi.org/10.1021/jacs.7b08345.

(68) Wang, X.; Conway, W.; Burns, R.; McCann, N.; Maeder, M. Comprehensive Study of the Hydration and Dehydration Reactions of Carbon Dioxide in Aqueous Solution. *J. Phys. Chem. A* **2010**, *114* (4), 1734–1740. https://doi.org/10.1021/jp909019u.

(69) Eigen, M.; De Maeyer, L. Self-Dissociation and Protonic Charge Transport in Water And. *Proc. R. Soc. Lond. A* **1958**, *247* (1251), 505–533. https://doi.org/10.1098/rspa.1958.0208.

(70) Hashiba, H.; Weng, L.-C.; Chen, Y.; Sato, H. K.; Yotsuhashi, S.; Xiang, C.; Weber, A. Z. Effects of Electrolyte Buffer Capacity on Surface Reactant Species and the Reaction Rate of CO_2 in Electrochemical CO_2 Reduction. *J. Phys. Chem. C* **2018**, *122* (7), 3719–3726. https://doi.org/10.1021/acs.jpcc.7b11316.

(71) Houle, F. A.; Hinsberg, W. D.; Sanchez, M. I.; Hoffnagle, J. A. Influence of Resist Components on Image Blur in a Patterned Positive-Tone Chemically Amplified Photoresist. *J. Vac. Sci. Technol. B* **2002**, *20* (3), 924. https://doi.org/10.1116/1.1475985.

(72) Tang, M. T.; Liu, X.; Ji, Y.; Norskov, J. K.; Chan, K. Modeling Hydrogen Evolution Reaction Kinetics through Explicit Water–Metal Interfaces. *J. Phys. Chem. C* **2020**, *124* (51), 28083–28092. https://doi.org/10.1021/acs.jpcc.0c08310.

(73) Chen, L. D.; Urushihara, M.; Chan, K.; Nørskov, J. K. Electric Field Effects in Electrochemical CO_2 Reduction. *ACS Catal.* **2016**, *6* (10), 7133–7139. https://doi.org/10.1021/acscatal.6b02299.

(74) Wise, D. L.; Houghton, G. Diffusion Coefficients of Neon, Krypton, Xenon, Carbon Monoxide and Nitric Oxide in Water at 10–60°C. *Chemical Engineering Science* **1968**, *23* (10), 1211–1216. https://doi.org/10.1016/0009-2509(68)89029-3.

(75) Simon, P. S.; Makita, H.; Bogacz, I.; Fuller, F.; Bhowmick, A.; Hussein, R.; Ibrahim, M.; Zhang, M.; Chatterjee, R.; Cheah, M. H.; Chernev, P.; Doyle, M. D.; Brewster, A. S.; Alonso-Mori, R.; Sauter, N. K.; Bergmann, U.; Dobbek, H.; Zouni, A.; Messinger, J.; Kern,

J.; Yachandra, V. K.; Yano, J. Capturing the Sequence of Events during the Water Oxidation Reaction in Photosynthesis Using XFELs. *FEBS Letters* **2023**, *597* (1), 30–37. https://doi.org/10.1002/1873-3468.14527.

(76) Shen, J.-R. The Structure of Photosystem II and the Mechanism of Water Oxidation in Photosynthesis. *Annu. Rev. Plant Biol.* **2015**, *66* (1), 23–48. https://doi.org/10.1146/annurev-arplant-050312-120129.

(77) Cordas, C. M.; Moura, J. J. G.; Escapa, A.; Mateos, R. Carbon Dioxide Utilization—Bioelectrochemical Approaches. In *Enzymes for Solving Humankind's Problems*; Moura, J. J. G., Moura, I., Maia, L. B., Eds.; Springer International Publishing: Cham, 2021; pp 83–108. https://doi.org/10.1007/978-3-030-58315-6_3.

(78) Maia, L. B.; Moura, I.; Moura, J. J. G. Carbon Dioxide Utilisation—The Formate Route. In *Enzymes for Solving Humankind's Problems*; Moura, J. J. G., Moura, I., Maia, L. B., Eds.; Springer International Publishing: Cham, 2021; pp 29–81. https://doi.org/10.1007/978-3-030-58315-6_2.

(79) Cordas, C. M.; Moura, J. J. G. Molybdenum and Tungsten Enzymes Redox Properties – A Brief Overview. *Coordination Chemistry Reviews* **2019**, *394*, 53–64. https://doi.org/10.1016/j.ccr.2019.05.005.

(80) Birrell, J. A.; Rodríguez-Maciá, P.; Reijerse, E. J.; Martini, M. A.; Lubitz, W. The Catalytic Cycle of [FeFe] Hydrogenase: A Tale of Two Sites. *Coordination Chemistry Reviews* **2021**, *449*, 214191. https://doi.org/10.1016/j.ccr.2021.214191.

(81) Einsle, O.; Rees, D. C. Structural Enzymology of Nitrogenase Enzymes. *Chem. Rev.* **2020**, *120* (12), 4969–5004. https://doi.org/10.1021/acs.chemrev.0c00067.

(82) Hoffman, B. M.; Lukoyanov, D.; Yang, Z.-Y.; Dean, D. R.; Seefeldt, L. C. Mechanism of Nitrogen Fixation by Nitrogenase: The Next Stage. *Chem. Rev.* **2014**, *114* (8), 4041–4062. https://doi.org/10.1021/cr400641x.

(83) Buscagan, T. M.; Rees, D. C. Rethinking the Nitrogenase Mechanism: Activating the Active Site. *Joule* **2019**, *3* (11), 2662–2678. https://doi.org/10.1016/j.joule.2019.09.004.

(84) Zhang, C.; Chen, C.; Dong, H.; Shen, J.-R.; Dau, H.; Zhao, J. A Synthetic Mn_4Ca-Cluster Mimicking the Oxygen-Evolving Center of Photosynthesis. *Science* **2015**, *348* (6235), 690–693. https://doi.org/10.1126/science.aaa6550.

(85) Hambourger, M.; Moore, G. F.; Kramer, D. M.; Gust, D.; Moore, A. L.; Moore, T. A. Biology and Technology for Photochemical Fuel Production. *Chem. Soc. Rev.* **2009**, *38* (1), 25–35. https://doi.org/10.1039/B800582F.

(86) Van Stappen, C.; Deng, Y.; Liu, Y.; Heidari, H.; Wang, J.-X.; Zhou, Y.; Ledray, A. P.; Lu, Y. Designing Artificial Metalloenzymes by Tuning of the Environment beyond the Primary Coordination Sphere. *Chem. Rev.* **2022**, *122* (14), 11974–12045. https://doi.org/10.1021/acs.chemrev.2c00106.

(87) Zhao, M.; Wang, H.-B.; Ji, L.-N.; Mao, Z.-W. Insights into Metalloenzyme Microenvironments: Biomimetic Metal Complexes with a Functional Second Coordination Sphere. *Chem. Soc. Rev.* **2013**, *42* (21), 8360. https://doi.org/10.1039/c3cs60162e.

(88) Jiao, L.; Wang, J.; Jiang, H.-L. Microenvironment Modulation in Metal–Organic Framework-Based Catalysis. *Acc. Mater. Res.* **2021**, *2* (5), 327–339. https://doi.org/10.1021/accountsmr.1c00009.

(89) Lewis, J. C. Beyond the Second Coordination Sphere: Engineering Dirhodium Artificial Metalloenzymes To Enable Protein Control of Transition Metal Catalysis. *Acc. Chem. Res.* **2019**, *52* (3), 576–584. https://doi.org/10.1021/acs.accounts.8b00625.

(90) Abdallah, W.; Hong, X.; Banta, S.; Wheeldon, I. Microenvironmental Effects Can Masquerade as Substrate Channelling in Cascade Biocatalysis. *Current Opinion in Biotechnology* **2022**, *73*, 233–239. https://doi.org/10.1016/j.copbio.2021.08.014.

(91) Ibrahim, M.; Fransson, T.; Chatterjee, R.; Cheah, M. H.; Hussein, R.; Lassalle, L.; Sutherlin, K. D.; Young, I. D.; Fuller, F. D.; Gul, S.; Kim, I.-S.; Simon, P. S.; de Lichtenberg, C.; Chernev, P.; Bogacz, I.; Pham, C. C.; Orville, A. M.; Saichek, N.; Northen, T.; Batyuk, A.; Carbajo, S.; Alonso-Mori, R.; Tono, K.; Owada, S.; Bhowmick, A.; Bolotovsky, R.; Mendez, D.; Moriarty, N. W.; Holton, J. M.; Dobbek, H.; Brewster, A. S.; Adams, P. D.; Sauter, N. K.; Bergmann, U.; Zouni, A.; Messinger, J.; Kern, J.; Yachandra,

V. K.; Yano, J. Untangling the Sequence of Events during the $S_2 \rightarrow S_3$ Transition in Photosystem II and Implications for the Water Oxidation Mechanism. *Proc. Natl. Acad. Sci. U.S.A.* **2020**, *117* (23), 12624–12635. https://doi.org/10.1073/pnas.2000529117.

(92) Suga, M.; Akita, F.; Yamashita, K.; Nakajima, Y.; Ueno, G.; Li, H.; Yamane, T.; Hirata, K.; Umena, Y.; Yonekura, S.; Yu, L.-J.; Murakami, H.; Nomura, T.; Kimura, T.; Kubo, M.; Baba, S.; Kumasaka, T.; Tono, K.; Yabashi, M.; Isobe, H.; Yamaguchi, K.; Yamamoto, M.; Ago, H.; Shen, J.-R. An Oxyl/Oxo Mechanism for Oxygen-Oxygen Coupling in PSII Revealed by an x-Ray Free-Electron Laser. *Science* **2019**, *366* (6463), 334–338. https://doi.org/10.1126/science.aax6998.

(93) Hussein, R.; Ibrahim, M.; Bhowmick, A.; Simon, P. S.; Chatterjee, R.; Lassalle, L.; Doyle, M.; Bogacz, I.; Kim, I.-S.; Cheah, M. H.; Gul, S.; de Lichtenberg, C.; Chernev, P.; Pham, C. C.; Young, I. D.; Carbajo, S.; Fuller, F. D.; Alonso-Mori, R.; Batyuk, A.; Sutherlin, K. D.; Brewster, A. S.; Bolotovsky, R.; Mendez, D.; Holton, J. M.; Moriarty, N. W.; Adams, P. D.; Bergmann, U.; Sauter, N. K.; Dobbek, H.; Messinger, J.; Zouni, A.; Kern, J.; Yachandra, V. K.; Yano, J. Structural Dynamics in the Water and Proton Channels of Photosystem II during the S2 to S3 Transition. *Nat Commun* **2021**, *12* (1), 6531. https://doi.org/10.1038/s41467-021-26781-z.

(94) Kern, J.; Chatterjee, R.; Young, I. D.; Fuller, F. D.; Lassalle, L.; Ibrahim, M.; Gul, S.; Fransson, T.; Brewster, A. S.; Alonso-Mori, R.; Hussein, R.; Zhang, M.; Douthit, L.; de Lichtenberg, C.; Cheah, M. H.; Shevela, D.; Wersig, J.; Seuffert, I.; Sokaras, D.; Pastor, E.; Weninger, C.; Kroll, T.; Sierra, R. G.; Aller, P.; Butryn, A.; Orville, A. M.; Liang, M.; Batyuk, A.; Koglin, J. E.; Carbajo, S.; Boutet, S.; Moriarty, N. W.; Holton, J. M.; Dobbek, H.; Adams, P. D.; Bergmann, U.; Sauter, N. K.; Zouni, A.; Messinger, J.; Yano, J.; Yachandra, V. K. Structures of the Intermediates of Kok's Photosynthetic Water Oxidation Clock. *Nature* **2018**, *563* (7731), 421–425. https://doi.org/10.1038/s41586-018-0681-2.

(95) Nevo, R.; Charuvi, D.; Tsabari, O.; Reich, Z. Composition, Architecture and Dynamics of the Photosynthetic Apparatus in Higher Plants: The Photosynthetic Apparatus in Higher Plants. *The Plant Journal* **2012**, *70* (1), 157–176. https://doi.org/10.1111/j.1365-313X.2011.04876.x.

(96) Alric, J.; Lavergne, J.; Rappaport, F. Redox and ATP Control of Photosynthetic Cyclic Electron Flow in Chlamydomonas Reinhardtii (I) Aerobic Conditions. *Biochimica et Biophysica Acta (BBA) - Bioenergetics* **2010**, *1797* (1), 44–51. https://doi.org/10.1016/j.bbabio.2009.07.009.

(97) Oung, H. M. O.; Mukhopadhyay, R.; Svoboda, V.; Charuvi, D.; Reich, Z.; Kirchhoff, H. Differential Response of the Photosynthetic Machinery to Dehydration in Older and Younger Resurrection Plants. *Journal of Experimental Botany* **2022**, *73* (5), 1566–1580. https://doi.org/10.1093/jxb/erab485.

(98) Suorsa, M. Cyclic Electron Flow Provides Acclimatory Plasticity for the Photosynthetic Machinery under Various Environmental Conditions and Developmental Stages. *Front. Plant Sci.* **2015**, *6*, 800. https://doi.org/10.3389/fpls.2015.00800.

(99) Kong, S.-G.; Wada, M. Molecular Basis of Chloroplast Photorelocation Movement. *J Plant Res* **2016**, *129* (2), 159–166. https://doi.org/10.1007/s10265-016-0788-1.

(100) Wada, M.; Kong, S.-G. Actin-Mediated Movement of Chloroplasts. *Journal of Cell Science* **2018**, *131* (2), jcs210310. https://doi.org/10.1242/jcs.210310.

(101) Kirchhoff, H. Chloroplast Ultrastructure in Plants. *New Phytol* **2019**, *223* (2), 565–574. https://doi.org/10.1111/nph.15730.

(102) Gu, L.; Grodzinski, B.; Han, J.; Marie, T.; Zhang, Y.; Song, Y. C.; Sun, Y. Granal Thylakoid Structure and Function: Explaining an Enduring Mystery of Higher Plants. *New Phytologist* **2022**, *236* (2), 319–329. https://doi.org/10.1111/nph.18371.

(103) Li, M.; Mukhopadhyay, R.; Svoboda, V.; Oung, H. M. O.; Mullendore, D. L.; Kirchhoff, H. Measuring the Dynamic Response of the Thylakoid Architecture in Plant Leaves by Electron Microscopy. *Plant Direct* **2020**, *4* (11), 00:1-14. https://doi.org/10.1002/pld3.280.

(104) Kirchhoff, H.; Hall, C.; Wood, M.; Herbstová, M.; Tsabari, O.; Nevo, R.; Charuvi, D.; Shimoni, E.; Reich, Z. Dynamic Control of Protein Diffusion within the Granal Thylakoid Lumen. *Proc. Natl. Acad. Sci. U.S.A.* **2011**, *108* (50), 20248–20253. https://doi.org/10.1073/pnas.1104141109.

(105) Kirchhoff, H. Structural Changes of the Thylakoid Membrane Network Induced by High Light Stress in Plant Chloroplasts. *Phil. Trans. R. Soc. B* **2014**, *369* (1640), 20130225. https://doi.org/10.1098/rstb.2013.0225.

(106) Barber, J. Photosynthetic Energy Conversion: Natural and Artificial. *Chem. Soc. Rev.* **2009**, *38* (1), 185–196. https://doi.org/10.1039/B802262N.

(107) Zhang, B.; Sun, L. Artificial Photosynthesis: Opportunities and Challenges of Molecular Catalysts. *Chem. Soc. Rev.* **2019**, *48* (7), 2216–2264. https://doi.org/10.1039/C8CS00897C.

(108) Yager, K. G.; Barrett, C. J. Novel Photo-Switching Using Azobenzene Functional Materials. *Journal of Photochemistry and Photobiology A: Chemistry* **2006**, *182* (3), 250–261. https://doi.org/10.1016/j.jphotochem.2006.04.021.

(109) Mahimwalla, Z.; Yager, K. G.; Mamiya, J.; Shishido, A.; Priimagi, A.; Barrett, C. J. Azobenzene Photomechanics: Prospects and Potential Applications. *Polym. Bull.* **2012**, *69* (8), 967–1006. https://doi.org/10.1007/s00289-012-0792-0.

(110) Kuenstler, A. S.; Clark, K. D.; Read de Alaniz, J.; Hayward, R. C. Reversible Actuation via Photoisomerization-Induced Melting of a Semicrystalline Poly(Azobenzene). *ACS Macro Lett.* **2020**, *9* (6), 902–909. https://doi.org/10.1021/acsmacrolett.0c00328.

(111) Dowds, M.; Bank, D.; Strueben, J.; Soto, D. P.; Sönnichsen, F. D.; Renth, F.; Temps, F.; Staubitz, A. Efficient Reversible Photoisomerisation with Large Solvodynamic Size-Switching of a Main Chain Poly(Azobenzene- *Alt* -Trisiloxane). *J. Mater. Chem. C* **2020**, *8* (5), 1835–1845. https://doi.org/10.1039/C9TC05193G.

(112) Andrew, T. L.; Tsai, H.-Y.; Menon, R. Confining Light to Deep Subwavelength Dimensions to Enable Optical Nanopatterning. *Science* **2009**, *324* (5929), 917–921. https://doi.org/10.1126/science.1167704.

(113) Warburton, R. E.; Soudackov, A. V.; Hammes-Schiffer, S. Theoretical Modeling of Electrochemical Proton-Coupled Electron Transfer. *Chem. Rev.* **2022**, *122* (12), 10599–10650. https://doi.org/10.1021/acs.chemrev.1c00929.

(114) Tyburski, R.; Liu, T.; Glover, S. D.; Hammarström, L. Proton-Coupled Electron Transfer Guidelines, Fair and Square. *J. Am. Chem. Soc.* **2021**, *143* (2), 560–576. https://doi.org/10.1021/jacs.0c09106.

(115) Gileadi, E. Simultaneous Two-Electron Transfer in Electrode Kinetics. *Journal of Electroanalytical Chemistry* **2002**, *532* (1–2), 181–189. https://doi.org/10.1016/S0022-0728(02)00766-0.

(116) Savéant, J.-M. Concerted Proton-Electron Transfers: Fundamentals and Recent Developments. *Annual Rev. Anal. Chem.* **2014**, *7* (1), 537–560. https://doi.org/10.1146/annurev-anchem-071213-020315.

(117) Reece, S. Y.; Nocera, D. G. Proton-Coupled Electron Transfer in Biology: Results from Synergistic Studies in Natural and Model Systems. *Annu. Rev. Biochem.* **2009**, *78* (1), 673–699. https://doi.org/10.1146/annurev.biochem.78.080207.092132.

(118) Koper, M. T. M. Theory of Multiple Proton–Electron Transfer Reactions and Its Implications for Electrocatalysis. *Chem. Sci.* **2013**, *4* (7), 2710. https://doi.org/10.1039/c3sc50205h.

(119) Zhou, T.; Huang, X.; Ding, N.; Lin, Z.; Yao, Y.; Guo, J. Porous Polyelectrolyte Frameworks: Synthesis, Post-Ionization and Advanced Applications. *Chem. Soc. Rev.* **2022**, *51* (1), 237–267. https://doi.org/10.1039/D1CS00889G.

(120) Houle, F. A. Adaptive Response by an Electrolyte: Resilience to Electron Losses in a Dye-Sensitized Porous Photoanode. *Chemical Science* **2021**, *12* (17), 6117–6128. https://doi.org/10.1039/D1SC00384D.

(121) Hussein, R.; Ibrahim, M.; Bhowmick, A.; Simon, P. S.; Chatterjee, R.; Lassalle, L.; Doyle, M.; Bogacz, I.; Kim, I.-S.; Cheah, M. H.; Gul, S.; de Lichtenberg, C.; Chernev, P.; Pham, C. C.; Young, I. D.; Carbajo, S.; Fuller, F. D.; Alonso-Mori, R.; Batyuk, A.; Sutherlin, K. D.; Brewster, A. S.; Bolotovsky, R.; Mendez, D.; Holton, J. M.; Moriarty, N. W.; Adams, P. D.; Bergmann, U.; Sauter, N. K.; Dobbek, H.; Messinger, J.; Zouni, A.; Kern, J.; Yachandra, V. K.; Yano, J. Structural Dynamics in the Water and Proton Channels of

Photosystem II during the S2 to S3 Transition. *Nat Commun* **2021**, *12* (1), 6531. https://doi.org/10.1038/s41467-021-26781-z.

(122) Bozal-Ginesta, C.; Mesa, C. A.; Eisenschmidt, A.; Francàs, L.; Shankar, R. B.; Antón-García, D.; Warnan, J.; Willkomm, J.; Reynal, A.; Reisner, E.; Durrant, J. R. Charge Accumulation Kinetics in Multi-Redox Molecular Catalysts Immobilised on TiO_2. *Chem. Sci.* **2021**, *12* (3), 946–959. https://doi.org/10.1039/D0SC04344C.

(123) Mesa, C. A.; Francàs, L.; Yang, K. R.; Garrido-Barros, P.; Pastor, E.; Ma, Y.; Kafizas, A.; Rosser, T. E.; Mayer, M. T.; Reisner, E.; Grätzel, M.; Batista, V. S.; Durrant, J. R. Multihole Water Oxidation Catalysis on Haematite Photoanodes Revealed by Operando Spectroelectrochemistry and DFT. *Nat. Chem.* **2020**, *12* (1), 82–89. https://doi.org/10.1038/s41557-019-0347-1.

(124) Song, W.; Ito, A.; Binstead, R. A.; Hanson, K.; Luo, H.; Brennaman, M. K.; Concepcion, J. J.; Meyer, T. J. Accumulation of Multiple Oxidative Equivalents at a Single Site by Cross-Surface Electron Transfer on TiO_2. *J. Am. Chem. Soc.* **2013**, *135* (31), 11587–11594. https://doi.org/10.1021/ja4032538.

(125) Amthor, S.; Knoll, S.; Heiland, M.; Zedler, L.; Li, C.; Nauroozi, D.; Tobaschus, W.; Mengele, A. K.; Anjass, M.; Schubert, U. S.; Dietzek-Ivanšić, B.; Rau, S.; Streb, C. A Photosensitizer–Polyoxometalate Dyad That Enables the Decoupling of Light and Dark Reactions for Delayed on-Demand Solar Hydrogen Production. *Nat. Chem.* **2022**, *14* (3), 321–327. https://doi.org/10.1038/s41557-021-00850-8.

(126) Kusoglu, A.; Weber, A. Z. New Insights into Perfluorinated Sulfonic-Acid Ionomers. *Chem. Rev.* **2017**, *117* (3), 987–1104. https://doi.org/10.1021/acs.chemrev.6b00159.

(127) Zhuang, T.-T.; Pang, Y.; Liang, Z.-Q.; Wang, Z.; Li, Y.; Tan, C.-S.; Li, J.; Dinh, C. T.; De Luna, P.; Hsieh, P.-L.; Burdyny, T.; Li, H.-H.; Liu, M.; Wang, Y.; Li, F.; Proppe, A.; Johnston, A.; Nam, D.-H.; Wu, Z.-Y.; Zheng, Y.-R.; Ip, A. H.; Tan, H.; Chen, L.-J.; Yu, S.-H.; Kelley, S. O.; Sinton, D.; Sargent, E. H. Copper Nanocavities Confine Intermediates for Efficient Electrosynthesis of C3 Alcohol Fuels from Carbon Monoxide. *Nat Catal* **2018**, *1* (12), 946–951. https://doi.org/10.1038/s41929-018-0168-4.

(128) Simon, G. H.; Kley, C. S.; Roldan Cuenya, B. Potential-Dependent Morphology of Copper Catalysts During CO_2 Electroreduction Revealed by In Situ Atomic Force Microscopy. *Angew. Chem. Int. Ed.* **2021**, *60* (5), 2561–2568. https://doi.org/10.1002/anie.202010449.

(129) Grosse, P.; Gao, D.; Scholten, F.; Sinev, I.; Mistry, H.; Roldan Cuenya, B. Dynamic Changes in the Structure, Chemical State and Catalytic Selectivity of Cu Nanocubes during CO_2 Electroreduction: Size and Support Effects. *Angew. Chem. Int. Ed.* **2018**, *57* (21), 6192–6197. https://doi.org/10.1002/anie.201802083.

(130) Pannwitz, A.; Klein, D. M.; Rodríguez-Jiménez, S.; Casadevall, C.; Song, H.; Reisner, E.; Hammarström, L.; Bonnet, S. Roadmap towards Solar Fuel Synthesis at the Water Interface of Liposome Membranes. *Chem. Soc. Rev.* **2021**, *50* (8), 4833–4855. https://doi.org/10.1039/D0CS00737D.

(131) Berger, A.; Segalman, R. A.; Newman, J. Material Requirements for Membrane Separators in a Water-Splitting Photoelectrochemical Cell. *Energy Environ. Sci.* **2014**, *7* (4), 1468–1476. https://doi.org/10.1039/C3EE43807D.

(132) Kistler, T. A.; Um, M. Y.; Cooper, J. K.; Sharp, I. D.; Agbo, P. Monolithic Photoelectrochemical CO_2 Reduction Producing Syngas at 10% Efficiency. *Adv. Energy Mater.* **2021**, *11* (21), 2100070. https://doi.org/10.1002/aenm.202100070.

(133) Miller, D. J.; Houle, F. A. Chapter 10. Membranes for Solar Fuels Devices. In *Energy and Environment Series*; Sharp, I. D., Atwater, H. A., Lewerenz, H.-J., Eds.; Royal Society of Chemistry: Cambridge, 2018; pp 341–385. https://doi.org/10.1039/9781788010313-00341.

(134) Low, Z.-X.; Budd, P. M.; McKeown, N. B.; Patterson, D. A. Gas Permeation Properties, Physical Aging, and Its Mitigation in High Free Volume Glassy Polymers. *Chem. Rev.* **2018**, *118* (12), 5871–5911. https://doi.org/10.1021/acs.chemrev.7b00629.

(135) Wijmans, J. G.; Baker, R. W. The Solution-Diffusion Model: A Review. *Journal of Membrane Science* **1995**, *107* (1–2), 1–21. https://doi.org/10.1016/0376-7388(95)00102-I.

(136) Perazio, A.; Lowe, G.; Gobetto, R.; Bonin, J.; Robert, M. Light-Driven Catalytic Conversion of CO2 with Heterogenized Molecular Catalysts Based on Fourth Period Transition Metals. *Coordination Chemistry Reviews* **2021**, *443*, 214018. https://doi.org/10.1016/j.ccr.2021.214018.

(137) Thevenon, A.; Rosas-Hernández, A.; Peters, J. C.; Agapie, T. In-Situ Nanostructuring and Stabilization of Polycrystalline Copper by an Organic Salt Additive Promotes Electrocatalytic CO_2 Reduction to Ethylene. *Angew. Chem. Int. Ed.* **2019**, *58* (47), 16952–16958. https://doi.org/10.1002/anie.201907935.

(138) Han, Z.; Kortlever, R.; Chen, H.-Y.; Peters, J. C.; Agapie, T. CO_2 Reduction Selective for $C_{\geq 2}$ Products on Polycrystalline Copper with N-Substituted Pyridinium Additives. *ACS Cent. Sci.* **2017**, *3* (8), 853–859. https://doi.org/10.1021/acscentsci.7b00180.

(139) Qu, P.; Cleveland, J. W.; Ahmed, E.; Liu, F.; Dubrawski, S.; Jones, C. W.; Weck, M. Compartmentalisation of Molecular Catalysts for Nonorthogonal Tandem Catalysis. *Chem. Soc. Rev.* **2022**, *51* (1), 57–70. https://doi.org/10.1039/D1CS00530H.

(140) Zou, N.; Zhou, X.; Chen, G.; Andoy, N. M.; Jung, W.; Liu, G.; Chen, P. Cooperative Communication within and between Single Nanocatalysts. *Nature Chem* **2018**, *10* (6), 607–614. https://doi.org/10.1038/s41557-018-0022-y.

(141) Wheeldon, I.; Minteer, S. D.; Banta, S.; Barton, S. C.; Atanassov, P.; Sigman, M. Substrate Channelling as an Approach to Cascade Reactions. *Nature Chem* **2016**, *8* (4), 299–309. https://doi.org/10.1038/nchem.2459.

(142) Zhang, Y.; Tsitkov, S.; Hess, H. Proximity Does Not Contribute to Activity Enhancement in the Glucose Oxidase–Horseradish Peroxidase Cascade. *Nat Commun* **2016**, *7* (1), 13982. https://doi.org/10.1038/ncomms13982.

(143) Hinzpeter, F.; Tostevin, F.; Buchner, A.; Gerland, U. Trade-Offs and Design Principles in the Spatial Organization of Catalytic Particles. *Nat. Phys.* **2022**, *18* (2), 203–211. https://doi.org/10.1038/s41567-021-01444-4.

TOC graphic